Biol. Cybern. 86, 209–230 (2002)
DOI 10.1007/s00422-001-0290-1

Biological Cybernetics

Using sensory weighting to model the influence of canal, otolith and visual cues on spatial orientation and eye movements

L. H. Zupan[1], **D. M. Merfeld**[1], **C. Darlot**[2]

[1] Jenks Vestibular Physiology Laboratory, Massachusetts Eye and Ear Infirmary, Department of Otology and Laryngology, Harvard Medical School, 243 Charles Street, Suite 421, Boston, MA 02114, USA
[2] Ecole Nationale Supérieure des Télécommunications, URA CNRS 820, Paris, France

Received: 20 September 2000 / Accepted in revised form: 28 September 2001

Abstract. The sensory weighting model is a general model of sensory integration that consists of three processing layers. First, each sensor provides the central nervous system (CNS) with information regarding a specific physical variable. Due to sensor dynamics, this measure is only reliable for the frequency range over which the sensor is accurate. Therefore, we hypothesize that the CNS improves on the reliability of the individual sensor outside this frequency range by using information from other sensors, a process referred to as "frequency completion." Frequency completion uses internal models of sensory dynamics. This "improved" sensory signal is designated as the "sensory estimate" of the physical variable. Second, before being combined, information with different physical meanings is first transformed into a common representation; sensory estimates are converted to intermediate estimates. This conversion uses internal models of body dynamics and physical relationships. Third, several sensory systems may provide information about the same physical variable (e.g., semicircular canals and vision both measure self-rotation). Therefore, we hypothesize that the "central estimate" of a physical variable is computed as a weighted sum of all available intermediate estimates of this physical variable, a process referred to as "multicue weighted averaging." The resulting central estimate is fed back to the first two layers. The sensory weighting model is applied to three-dimensional (3D) visual–vestibular interactions and their associated eye movements and perceptual responses. The model inputs are 3D angular and translational stimuli. The sensory inputs are the 3D sensory signals coming from the semicircular canals, otolith organs, and the visual system. The angular and translational components of visual movement are assumed to be available as separate stimuli measured by the visual system using retinal slip and image deformation. In addition, both tonic ("regular") and phasic ("irregular") otolithic afferents are implemented. Whereas neither tonic nor phasic otolithic afferents distinguish gravity from linear acceleration, the model uses tonic afferents to estimate gravity and phasic afferents to estimate linear acceleration. The model outputs are the internal estimates of physical motion variables and 3D slow-phase eye movements. The model also includes a smooth pursuit module. The model matches eye responses and perceptual effects measured during various motion paradigms in darkness (e.g., centered and eccentric yaw rotation about an earth-vertical axis, yaw rotation about an earth-horizontal axis) and with visual cues (e.g., stabilized visual stimulation or optokinetic stimulation).

Correspondence to: L. H. Zupan

1 Introduction

Body movements stimulate sense organs, yielding sensory signals (e.g., signals from the semicircular canals, otolith organs and visual system) that encode motion and orientation. Despite limitations due to sensor dynamics and neural "noise", the central nervous system (CNS) is capable of accurately estimating motion and orientation under most conditions, a process referred to as multisensory integration. These various estimates of motion and orientation are then utilized, with additional motor and cognitive processing, to elicit reflexive and perceptual responses.

To stabilize the image of the external world on the retina, the CNS principally utilizes sensory signals coming from the vestibular (i.e., semicircular canals and otolith organs) and visual systems to elicit compensatory reflexive eye movements. By use of vestibular information, the vestibulo-ocular reflexes (VOR) help stabilize the image of the external world on the retina in response to head movements. By use of visual information, the optokinetic reflexes help stabilize the image of the external world on the retina in response to movements of the visual surround.

In this paper, we will model physical and physiological phenomena with mathematical tools. We attempt to describe reality with this model but do not confuse

model and reality. However, we do explicitly hypothesize that the CNS implements neural processes between groups of neurons equivalent to mathematical operations between central estimates of physical variables.

This paper presents a general model of human multisensory integration, the "sensory weighting" model, that unifies various previous approaches in a single model: feedback-loop control (Hain 1986; Robinson 1977; Schmid et al. 1980, 1979), "velocity storage integrator" (Raphan and Sturm 1991; Raphan et al. 1977; Wearne et al. 1999), "observer" (Glasauer 1992, 1993; Glasauer and Merfeld 1997; Merfeld 1990, 1995a; Merfeld et al. 1993a; Oman 1982), and "coherence constraint" (Droulez and Darlot 1989; Zupan 1995; Zupan et al. 1994) models. The sensory weighting model consists of three processing layers:

1. **Frequency completion.** The resulting sensory estimate is improved with respect to the sensor output by using an internal estimate, which is ideally accurate in the absence of noise and thus provides the missing information. Frequency completion uses internal models[1] of sensor dynamics.
2. **Conversion of sensory estimates to intermediates estimates.** Information with different physical meanings is transformed into a common representation (e.g., information about change of gravity is transformed into angular velocity). These transformations use internal models of physical relationships.
3. **Multicue weighted averaging of the intermediate estimates.** Weighted averaging is a Bayesian maximum-likelihood estimate with each weight being proportional to the inverse variance of the respective intermediate estimate. Thus, the free parameters of the model are mainly determined by the assumed variances of the respective intermediate estimates. The resulting central estimate is fed back to the first two layers.

Steps 1 and 2 are both necessary prerequisites for the weighted averaging. Frequency completion has to be performed to overcome the different sensor characteristics which would prohibit the use of weighted averaging (e.g., a low-pass-filtered estimate and a high-pass-filtered estimate of the same physical variable cannot be fused by weighted averaging). Conversion of sensory estimates to intermediate estimates is necessary since only variables having the same dimension can be fused by weighted averaging (e.g., a gravity estimate cannot be fused with an angular velocity estimate).

Internal models of sensory dynamics, body dynamics and physical relationships were also included in previous models of sensory integration (Droulez and Darlot 1989; Glasauer 1992, 1993; Glasauer and Merfeld 1997; Merfeld 1990, 1995a,b; Merfeld et al. 1993a; Zupan 1995) and motor control (Darlot et al. 1996; Kawato et al. 1987; Wolpert et al. 1995; Zupan 1995). But the "sensory weighting" model of visual–vestibular interactions is innovative and original when compared to previous approaches. First, the sensory weighting model implements visual–vestibular interactions while observer models have been limited to vestibular interactions. Second, the sensory weighting model implements an efference copy of the eye motor command similarly to the coherence constraint model (Droulez and Darlot 1989), as originally suggested by Von Holst and Mittelstaedt (1950). Third, whereas neither tonic ("regular") nor phasic ("irregular") otolithic afferents distinguish gravity from linear acceleration (Anderson et al. 1978; Fernandez and Goldberg 1976a; Loe et al. 1973), the model uses tonic afferent signals to estimate gravity, and phasic afferent signals to estimate linear acceleration, as previously suggested (Droulez and Darlot 1989; Mayne 1974; Young and Meiry 1968). Fourth, the sensory weighting model implements an idiotropic vector (Mittelstaedt 1983) to help estimate head orientation and motion.

2 Model description

2.1 Background and development

The sensory weighting model consists of three processing layers and proposes a solution to the problem of how the central (CNS) integrates sensory information from disparate sensory modalities to estimate body motion and spatial orientation. The sensory weighting model is the mathematical implementation of three hypotheses. First, we hypothesize that a physical variable is represented by two types of estimates in the CNS: a sensory estimate and a central estimate. Second, we hypothesize that internal models of sensory dynamics, body dynamics and physical relationships are implemented in the CNS to help calculate these two estimates of physical variables. Third, we hypothesize that the central estimate of a physical variable is computed by "multicue weighted averaging" of available sensory information. The basis for these hypotheses is presented in Sect. 4.

2.2 The physical variables

In the sensory weighting model, physical variables are represented by three-dimensional (3D) vectors in a right-handed orthogonal head-fixed frame of reference (x, y, z) where the x-, y-, and z-axes are the naso-occipital, interaural and rostrocaudal axes with positive values forward, to the left, and to the top of the head, respectively. For rotation, the x-, y-, and z-axes represent roll, pitch, and yaw rotations with positive values clockwise, downward, and to the left, respectively.

Similarly, internal estimates of physical variables are expressed in head-fixed frames of reference, as observed

[1] An internal model mimics a physical process (e.g., sensory dynamics, body dynamics, and the relationship between physical variables). If this physical process can be described by a mathematical operation between physical variables, an internal model really signifies that a neural process equivalent to this mathematical operation may occur within the groups of neurons that encode the internal estimates of these physical variables.

experimentally in several species (Graf et al. 1988; Krapp and Hengstenberg 1996; Wylie et al. 1998; Wylie and Frost 1993). 3D physical variables[2] considered are the head angular velocity ω, eye angular velocity in space r, eye angular velocity in head e, specific gravito-inertial force f, gravity g, head linear acceleration a, and head linear velocity v. To define optokinetic stimuli, we consider the angular (r_v) and linear (v_v) velocities of the vzisual surround in space in a space-fixed frame of reference.

The vestibular system is composed of the semicircular canals and otolith organs. The semicircular canals measure head angular velocity ω in a head-fixed frame of reference. The otolith organs, innervated by both tonic (''regular'') and phasic (''irregular'') otolithic afferents, measure the specific gravito-inertial force[3] f in a head-fixed frame of reference.

The study of the central processing that separates angular and translational information from visual flow is not central to this paper. Therefore, we assume for simplification that the visually estimated eye angular velocity in space (r_e) and head linear velocity in space (v_e) are available as independent inputs (Droulez and Darlot 1989). (For details on optic flow processing, see Droulez and Cornilleau-Pérès (1993) and Simpson (1984).) The visually estimated eye angular velocity in space r_e is chosen opposite the retinal slip and the visually estimated head linear velocity in space v_e results from the processing of image deformation. Finally, a measure of the eye angular velocity in head e is available to the CNS as an efference copy $\hat{e}_M$ of the motor order e_M sent to the motoneurons innervating the eye muscles, as suggested by Von Holst and Mittelstaedt (1950). Sensor and effector implementation is detailed in Appendix A.

During head rotation, a simple set of equations describes body dynamics and physical relationships that link the various physical variables in the head-fixed frame of reference:

$$dg/dt = g \times \omega \tag{1}$$

$$r = \omega + e \tag{2}$$

$$dv/dt = a - \omega \times v \tag{3}$$

$$f = g - a \tag{4}$$

where $\times$ designates the cross product of two vectors. Equations (1) and (3) are first-order differential equations that model the influence of head angular velocity ω on the relative orientation of gravity g, head translatory acceleration a, and head translatory velocity v. Note that the systems described by (1) and (3) with ω as input and g or v as output are non-linear systems, since linear superposition does not hold for the responses to two arbitrary inputs ω. Integration of these two equations is performed with initial values corresponding to head orientation and motion at the beginning of a simulation. (For similar differential equations between neural estimates, estimates of head orientation and motion at the beginning of a simulation are used for initial values.) These two equations were obtained directly from the mathematical relationship between time derivative operators in a moving (head) and fixed (external world) frames of reference (Spiegel 1972). For example, (1) mathematically describes how gravity is pitched forward in a head-fixed frame of reference when the head is pitched forward. As an approximation, head and eye rotation axes are considered identical, leading to the simple relationship (2). Finally, as stated by Einstein's equivalence principle, linear accelerometers like the otolith organs cannot distinguish gravity g from head linear acceleration a, but measure the gravito-inertial force f defined by (4).

2.3 A simple case: two sensors

In the Laplace frequency domain, a physical variable x_1 is measured by a sensor whose dynamics can be characterized by a transfer function matrix $\mathbf{T}_1(s)$ where s is the standard Laplace variable (Hildebrand 1976). While measured by one sensor, the physical variable x_1 may also be estimated using other available sensory information correlated with x_1. For example, semicircular canals do not accurately measure head angular velocity at low frequencies (<0.05 Hz). Therefore, to compute an estimate of head angular velocity over a broader frequency range, the CNS may also use visual information that principally contains low-frequency information. This has been confirmed by neural recordings (Fredrickson and Schwartz 1979; Waespe and Henn 1977, 1979) and illusory sensations of self-rotation (Dichgans et al. 1972).

The sensory weighting hypothesis states that the CNS uses all available sensory information to compute a central estimate $\hat{x}_1$ of the physical variable x_1. Figure 1 describes how the CNS computes a sensory estimate $\tilde{x}_1$ and a central estimate $\hat{x}_1$ of the physical variable x_1 (e.g., head angular velocity) given two sensory inputs (e.g., semicircular canal and visual inputs):

$$\tilde{x}_1 \equiv \mathbf{T}_1 x_1 + \left(\mathbf{I} - \hat{\mathbf{T}}_1\right)\hat{x}_1 \equiv \widehat{x}_{1,1} \tag{5}$$

$$\hat{x}_1 \equiv W_{1,1}\widehat{x}_{1,1} + W_{1,2}\widehat{x}_{1,2} \tag{6}$$

[2]Since all variables are expressed in a head-fixed frame of reference, some variables may be independent of head orientation. For example, yaw head angular velocity ω is always aligned with the head z-axis during a yaw rotation about either an earth-vertical or earth-horizontal axis.

[3] For a gravito-inertial force F acting on a body of mass m, the specific gravito-inertial force $f = F/m$ corresponds to the gravito-inertial force normalized by the mass m. The specific gravito-inertial force f is the sum of the specific gravitational (g) and inertial ($f_a = -a$) forces where g and a designate gravity and head linear acceleration, respectively. Therefore, $f = g - a$.

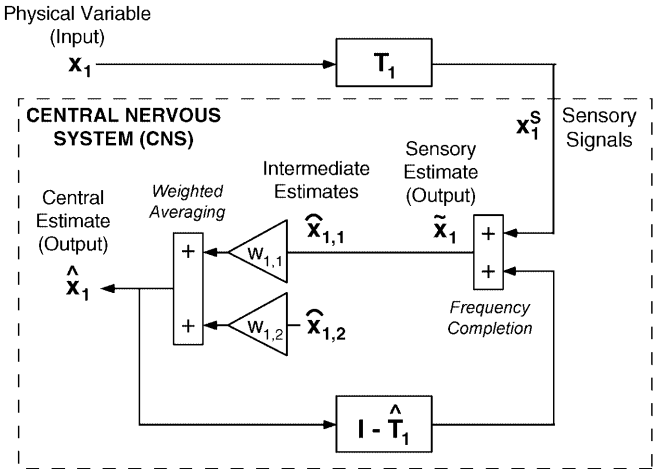

Fig. 1. Neural computation of a central estimate. The *solid lines* represent pathways that encode three-dimensional (3D) variables and the *dashed box* represents the central nervous system (CNS). Let x_1 designate a 3D physical variable. The dynamics of a sensor measuring the stimulus x_1 can be characterized by a transfer function matrix $\mathbf{T}_1$. Using an internal model of sensory dynamics ($\hat{\mathbf{T}}_1$) in a neural feedback loop, the sensory measurement x_1^S of the 3D physical variable x_1 is completed to yield a sensory estimate $\tilde{x}_1$, a process referred to as "frequency completion." ($\mathbf{I}$ is the 3D identity transfer function with $\mathbf{I}x = x$.) We consider two intermediate estimates $\widehat{x}_{1,1}$ and $\widehat{x}_{1,2}$ of the physical variable x_1. We hypothesize that the central estimate $\hat{x}_1$ of the physical variable x_1 is the weighted sum of the two intermediate estimates $\widehat{x}_{1,1}$ and $\widehat{x}_{1,2} (0 \leq W_{1,1} < 1$ and $0 \leq W_{1,2} < 1)$, a process referred to as "weighted averaging." (By definition, the intermediate estimate $\widehat{x}_{1,1}$ is equal to the sensory estimate $\tilde{x}_1$.)

In the sensory weighting model, the transfer function $\hat{\mathbf{T}}_1$ is referred to as an internal model of the sensory dynamics, since $\hat{\mathbf{T}}_1$ is generally chosen so that $\hat{\mathbf{T}}_1 = \mathbf{T}_1$. The transfer function $\mathbf{I} - \hat{\mathbf{T}}_1$ is referred to as an internal model of the complementary dynamics of the sensor. Indeed, if $\hat{\mathbf{T}}_1 = \mathbf{T}_1$ is a first-order high-pass filter with a time constant τ (e.g., semicircular canals) $\mathbf{I} - \hat{\mathbf{T}}_1$ is the complementary low-pass filter with the same time constant τ; similarly, if $\hat{\mathbf{T}}_1 = \mathbf{T}_1$ is a first-order low-pass filter with a time constant τ (e.g., part of the visual system that measures retinal slip), $\mathbf{I} - \hat{\mathbf{T}}_1$ is the complementary high-pass filter with the same time constant τ. Therefore, we will refer to (5) as the "frequency completion" mechanism. (As discussed in Appendix B, a low-pass filter is added to avoid algebraic feedback loops when $\hat{\mathbf{T}}_1$ is a low-pass filter.)

To perform the frequency completion, the central estimate $\hat{x}_1$ of the physical variable x_1 is fed back. This central estimate obtained as described in (6) by "multi-cue weighted averaging" of the intermediate estimates: weighted averaging is a Bayesian maximum-likelihood estimate with each weight being proportional to the inverse variance of the respective intermediate estimate. Thus, the free parameters of the model are mainly determined by the assumed variances of the respective intermediate estimates $\widehat{x}_{1,1}$ ($\widehat{x}_{1,1}$ equals $\tilde{x}_1$ by definition) and $\widehat{x}_{1,2}$ (e.g., $\widehat{x}_{1,2}$ may be obtained by processing sensory signals from the part of the visual system that measures retinal slip).

The sensory ($\tilde{x}_1$) and central ($\hat{x}_1$) estimates defined by (5) and (6) have different dynamics (see Appendix B for details). However, by use of an internal model of sensory dynamics, the bandwidth of both estimates has been augmented when compared to the sensory signal:

1. If the sensor is a high-pass filter (e.g., semicircular canals), both internal estimates are primarily high-pass-filtered versions of x_1, and the corresponding high-pass filter time constant is increased by a factor of $1/(1 - W_{1,1})$ compared to the sensor signal, leading to a larger high-pass bandwidth.
2. If the sensor is a low-pass filter (e.g., part of the visual system that measures retinal slip), both internal estimates are primarily low-pass-filtered versions of x_1, and the corresponding low-pass filter time constant is decreased by a factor of $(1 - W_{1,1})$ compared to the sensor signal, leading to a larger low-pass bandwidth.

If $\hat{\mathbf{T}}_1 = \mathbf{T}_1$, ideally accurate sensory ($\tilde{x}_1$) and central ($\hat{x}_1$) estimates are obtained in the absence of noise for $W_{1,1} + W_{1,2} = 1$.

2.4 The general case

The previous elementary scheme is generalized to a set of n physical variables x_i $(i = 1, \ldots, n)$, but the estimation process is outlined only for one physical variable x_i (Fig. 2). Using internal models of sensory dynamics, the sensory measurement x_i^S of the physical variable x_i is completed to yield a sensory estimate $\tilde{x}_i$ as outlined in Fig. 1. Using internal models of body dynamics and physical relationships, information with different physical meanings is transformed into a common representation (e.g., information about change of gravity is transformed into angular velocity). Therefore, sensory estimates $\tilde{x}_i$ $(i = 1, \ldots, n)$ are processed to yield intermediate estimates $\widehat{x}_{i,j}$ $(j = 1, \ldots, m; m \leq n)$, a process referred to as "estimate conversion": there are m intermediate estimates through multi-cue weighted averaging (for a review see (Howard 1997)) as the weighted sum of all intermediate estimates $\widehat{x}_{i,j}$ $(j = 1, \ldots, m; m \leq n)$ of the physical variable x_i:

$$\hat{x}_i \equiv \sum_{j=1}^{m} W_{i,j} \widehat{x}_{i,j} \tag{7}$$

where m is the number of intermediate estimates for a given physical variable, and n is the number of physical variables. The weighting parameters $W_{i,j}$ are defined as positive real scalars less than one $(0 < W_{i,j} \leq 1)$. The sensory ($\tilde{x}_i$) and central ($\hat{x}_i$) estimates of the physical variables x_i are combined by use of a scheme similar to the one described in Fig. 1:

$$\tilde{x}_i \equiv \mathbf{T}_i x_i + \left[\mathbf{I} - \hat{\mathbf{T}}_i\right] \hat{x}_i \equiv \widehat{x}_{i,i} \tag{8}$$

For $j = i$, the internal model relating the sensory estimate $\tilde{x}_i$ and the intermediate estimate $\widehat{x}_{i,i}$ is the

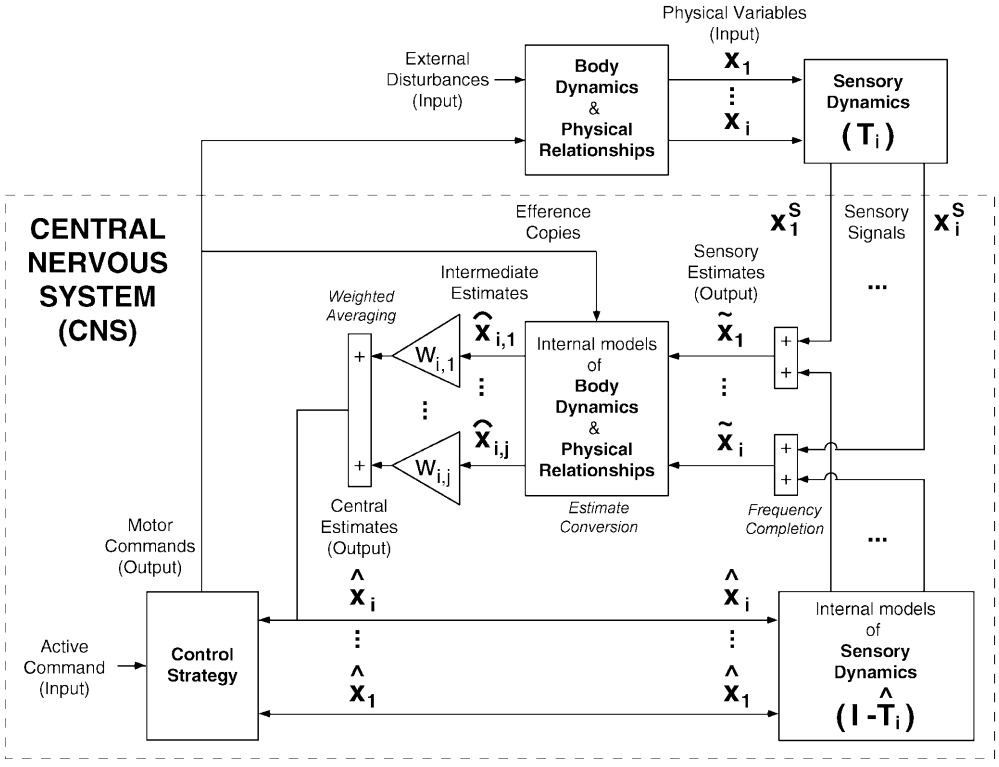

Fig. 2. Schematic representation of the sensory weighting model. The simple pattern shown in Fig. 1 is generalized to a set of n different physical variables x_i measured by n sensors ($\mathbf{T}_i$). The *solid lines* represent pathways that encode 3D variables and the *dashed box* represents the CNS. The three layers of the model are outlined. First, using internal models of sensory dynamics ($\hat{\mathbf{T}}_i$), the sensory measurement x_i^S of the 3D physical variable x_i is completed to yield a sensory estimate $\tilde{x}_i$, a process referred to as "frequency completion." Second, using internal models of body dynamics and physical relationships, the various sensory estimates $\tilde{x}_i$ $(i = 1, \ldots, n)$ are processed to yield various intermediate estimates $\widehat{x}_{i,j}$ of the physical variable x_i (by definition, $\widehat{x}_{i,i} \equiv \tilde{x}_i$), a process referred to as "estimate conversion." Third, these various estimates $\widehat{x}_{i,j}$ are weighted ($W_{i,j}$) and summed to yield the central estimate $\hat{x}_i$ of the physical variable x_i, a process referred to as "weighted averaging." The central estimate $\hat{x}_i$ is used to complete the sensory measurement x_i^S and to yield a sensory estimate $\tilde{x}_i$ of the physical variable x_i. Sensory estimates $\tilde{x}_i$, central estimates $\hat{x}_i$ and motor commands are the model outputs

identity operator. Therefore, the intermediate estimate $\widehat{x}_{i,i}$ equals the sensory estimate $\tilde{x}_i$.

2.5 The sensory weighting model

Figure 3 shows a block diagram of the sensory weighting model of visual–vestibular interactions. Switches S1 and S2 are closed when the visual system is active, and switch S3 is closed when smooth pursuit is active. In darkness, all switches are open (Appendix C).

In the sensory weighting model, gravity is preferentially estimated using sensory information from the tonic otolithic afferents and the semicircular canals. Head angular velocity ω and gravity g are linked by the nonlinear differential equation (1). This differential equation can be used to estimate gravity g by use of the head angular velocity ω:

$$g = \int (g \times \omega)\mathrm{d}t \tag{9}$$

We hypothesize that the CNS contains internal models of body dynamics and physical relationships (1–4). Using an internal model describing how head angular velocity ω and gravity g interact as in (9), the CNS computes the central estimates of gravity $\hat{g}$ by multicue averaging as in (7):

$$\hat{g} \equiv W_{\mathrm{g},1}\widehat{g}_1 + W_{\mathrm{g},2}\widehat{g}_2 = W_{\mathrm{g},1}\tilde{g} + W_{\mathrm{g},2}\int (\tilde{g} \times \tilde{\omega})\mathrm{d}t \tag{10}$$

where the sensory weights ($W_{g,1}$ and $W_{g,2}$) are between zero and one. The intermediate estimate of gravity $\widehat{g}_1$ equals the sensory estimate[4] $\tilde{g}$.

Reciprocally, in the sensory weighting model the head angular velocity can be estimated using sensory information from the otolith organs. By applying to both sides of (1) a cross product with an arbitrary vector u, head angular velocity ω can be expressed as a function of gravity g:

$$\begin{aligned} &\mathrm{d}g/\mathrm{d}t \times u = (g \times \omega) \times u \\ &\Rightarrow \omega = \frac{[\mathrm{d}g/\mathrm{d}t \times u + \langle \omega, u \rangle g]}{\langle g, u \rangle} \end{aligned} \tag{11}$$

[4] In the rest of the paper, the variables considered (ω, r, e, g, a, v) are differentiated by their names, rather than by using indices i as in Sect. 2.4. Therefore, from now on, indices are only used to differentiate intermediate estimates like the indices j in Sect. 2.4. According to (5), we have: $\widehat{\omega}_1 = \tilde{\omega}, \widehat{r}_1 = \tilde{r}, \widehat{g}_1 = \tilde{g}, \widehat{a}_1 = \tilde{a}$, and $\widehat{v}_1 = \tilde{v}$.

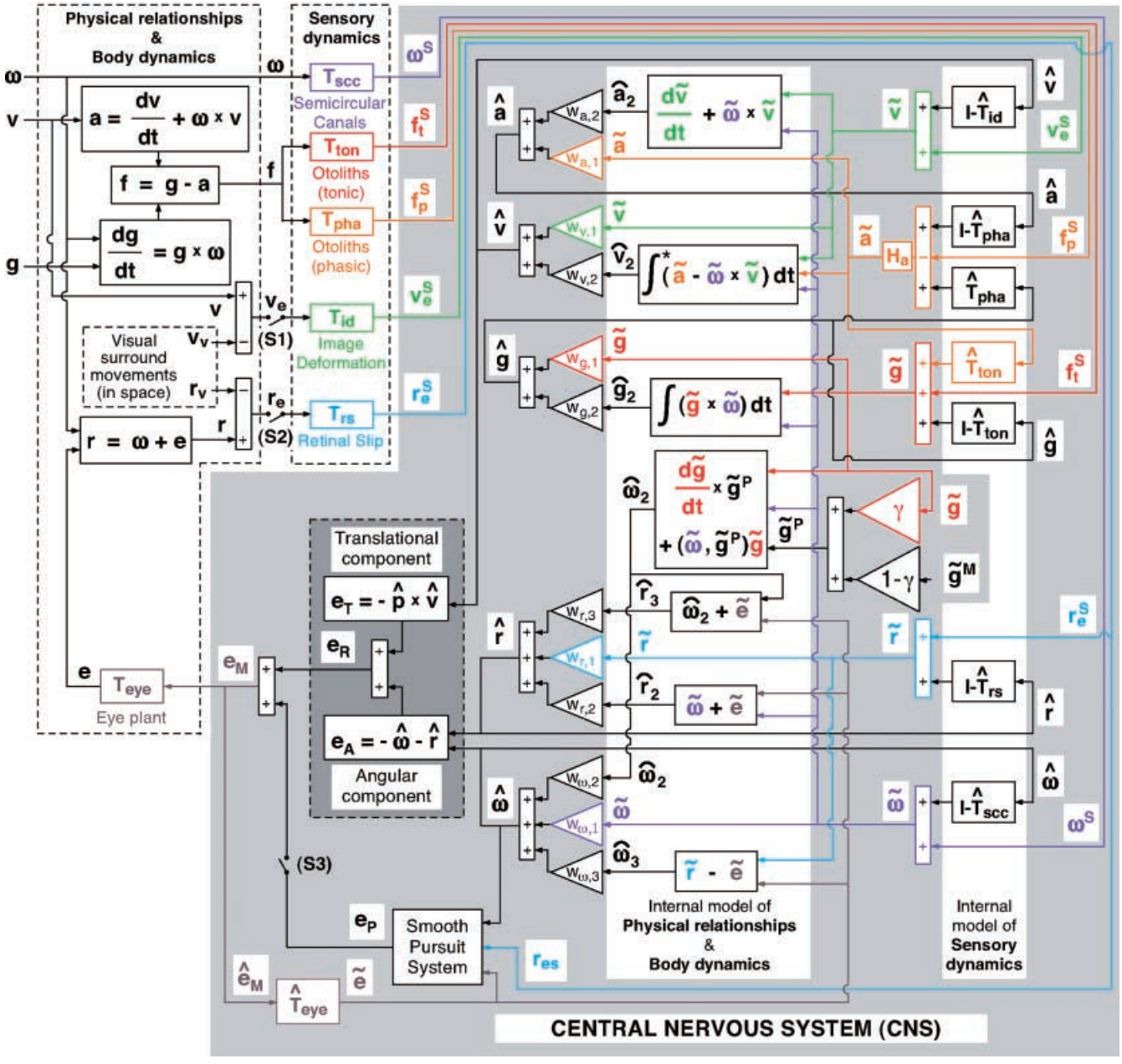

where $\langle\,,\rangle$ is the dot product (also known as inner product) of two vectors. This new relationship between head angular velocity ω and gravity g can be used to estimate head angular velocity by use of otolith information. Assuming $u = \tilde{g}^{\mathrm{P}}$ (see Eq. 13 below) and neglecting the scaling factor $1/\langle \tilde{g}, \tilde{g}^{\mathrm{P}} \rangle$ for simplification since it is equal to 1 in an upright orientation, an intermediate estimate of head angular velocity $\tilde{\omega}_2$ can be defined:

$$\tilde{\omega}_2 \equiv \mathrm{d}g/\mathrm{d}t \times \tilde{g}^{\mathrm{p}} + \langle \tilde{\omega}, \tilde{g}^{\mathrm{p}} \rangle \tilde{g} \tag{12}$$

$\tilde{g}^{\mathrm{P}}$ is a second sensory estimate of gravity defined as follows:

$$\tilde{g}^{\mathrm{P}} \equiv \gamma \tilde{g} + (1-\gamma)\tilde{g}^{\mathrm{M}} \tag{13}$$

where $\tilde{g}^{\mathrm{M}} = [0, 0, -1]$ (in units of G) is the idiotropic vector aligned with the rostrocaudal axis and γ is a real number between zero and one. Justification at this is presented in Sect. 4.

The sensory weighting model also processes visual information. The head angular velocity ω, slow-phase eye angular velocity in head e, and eye angular velocity in space r are linked by the mathematical relationship given in (2). By manipulating this relationship, another intermediate estimate of head angular velocity $\tilde{\omega}_3$ can be defined:

$$\tilde{\omega}_3 = \tilde{r} - \tilde{e} \tag{14}$$

Using internal models of body dynamics and physical relationships describing how gravity g, head angular

◀

Fig. 3. Block diagram model of compensatory reflexive eye movements during movements of the head and visual surround. To define visual surround motion, we consider the 3D angular velocity (r_v) and translational velocity (v_v) of the visual surround in space. To define head motion and orientation, we consider in a head-fixed frame of reference the 3D head angular velocity ω, eye angular velocity in space r, eye angular velocity in head e, gravity g, head linear acceleration a, and head linear velocity in space v. (We also define the gravito-inertial force $f = g - a$.) These physical variables are measured by various sensors, the dynamics of which are mathematically implemented by Laplace transfer functions ($\mathbf{T}_{scc}, \mathbf{T}_{ton}, \mathbf{T}_{pha}, \mathbf{T}_{id}, \mathbf{T}_{rs}$). The outputs of the model are the sensory estimates ($\tilde{\omega}, \tilde{r}, \tilde{e}, \tilde{g}, \tilde{a}, \tilde{v}$) and central estimates ($\hat{\omega}, \hat{r}, \hat{e}_M, \hat{g}, \hat{a}, \hat{v}$) of physical variables. Intermediate estimates $\widehat{\omega}_2$, $\widehat{\omega}_3$, $\widehat{r}_2$, $\widehat{r}_3$, $\widehat{g}_2$, $\widehat{v}_2$, $\widehat{a}_2$) are also computed. An additional sensory estimate $\tilde{g}^P$ is computed using the sensory estimate of gravity $\tilde{g}$ and the idiotropic vector $\tilde{g}^M = [0, 0, -1]$ in G units. To easily track afferent information, we represent the semicircular canal sensory signal and associated sensory estimate of head angular velocity in space $\tilde{\omega}$ in *magenta*, the tonic otolith afferent signal and associated sensory estimate of gravity $\tilde{g}$ in *red*, the phasic otolith afferent signal and associated sensory estimate of linear acceleration $\tilde{a}$ in *orange*, the visual image deformation signal and associated sensory estimate of linear velocity $\tilde{v}$ in *green*, and the visual retinal slip signal and associated sensory estimate of eye angular velocity in space $\tilde{r}$ in *blue*. In addition, we represent the efferent copy of the eye motor order $\hat{e}_M$ and associated sensory estimate of eye angular velocity in head $\tilde{e}$ in *brown*. Finally, when sensory estimates are combined to elicit intermediary sensory estimates and central estimates, we use the neutral color black, as for the rest of the figure. Sensory estimates are calculated using internal models of sensory dynamics ($\hat{\mathbf{T}}_{scc}, \hat{\mathbf{T}}_{ton}, \hat{\mathbf{T}}_{pha}, \hat{\mathbf{T}}_{id}, \hat{\mathbf{T}}_{rs}$) and body dynamics ($\hat{\mathbf{T}}_{eye}$). Internal models of physical relationships process the sensory estimates to elicit the central estimates. (Two additional operators were defined: a first-order high-pass filter $\mathbf{H}_a$ with a time constant $\tau_i = 200$ s and a first-order leaky-integrator $\int^* dt$ with a time constant $\tau_a = 0.13$ s.) The model also computes the eye angular velocity in head e, which is the eye response to the various eye command components: the angular (e_A), translational (e_T) and total (e_R) reflexive eye commands, the pursuit eye command e_P and the total eye command e_M. An efference copy of the total command $\hat{e}_M$ and a sensory estimate of the eye angular velocity in head $\tilde{e}$ are also computed. In darkness, the external visual feedback loop is open (switches S1 and S2 open), and the smooth pursuit system is deactivated (switch S3 open). In lighted conditions, switches S1, S2 and S3 are closed

velocity ω, eye angular velocity in head e, and eye angular velocity in space r interact as in (11) and (14), the CNS computes a central estimate of head angular velocity $\hat{\omega}$ by multicue averaging as in (7):

$$\hat{\omega} \equiv W_{\omega,1}\widehat{\omega}_1 + W_{\omega,2}\widehat{\omega}_2 + W_{\omega,3}\widehat{\omega}_3 \equiv W_{\omega,1}\tilde{\omega} + W_{\omega,2}(\mathrm{d}\tilde{g}/\mathrm{d}t \times \tilde{g}^p + \langle\tilde{\omega}, \tilde{g}^p\rangle\tilde{g}) + W_{\omega,3}(\tilde{r} - \tilde{e}) \quad (15)$$

where the sensory weights ($W_{\omega,1}$, $W_{\omega,2}$ $W_{\omega,3}$) are between zero and one. Similarly, the CNS computes a central estimate of eye angular velocity in space $\hat{r}$:

$$\hat{r} \equiv W_{r,1}\widehat{r}_1 + W_{r,2}\widehat{r}_2 + W_{r,3}\widehat{r}_3 \equiv W_{r,1}\tilde{r} + W_{r,2}(\tilde{\omega} + \tilde{e}) + W_{r,3}[(\mathrm{d}\tilde{g}/\mathrm{d}t \times \tilde{g}^p + \langle\tilde{\omega}, \tilde{g}^p\rangle\tilde{g}) + \tilde{e}] \quad (16)$$

where the sensory weights ($W_{r,1}$, $W_{r,2}$ $W_{r,3}$) are between zero and one.

Finally, using internal models of body dynamics and physical relationships describing how head angular velocity ω, linear acceleration a, and linear velocity v interact as in (3), the CNS computes central estimates of both linear acceleration $\hat{a}$ and linear velocity $\hat{v}$:

$$\hat{a} \equiv W_{a,1}\widehat{a}_1 + W_{a,2}\widehat{a}_2 = W_{a,1}\tilde{a} + W_{a,2}(\mathrm{d}\tilde{v}/\mathrm{d}t + \tilde{\omega} \times \tilde{v}) \quad (17)$$

$$\hat{\mathbf{v}} \equiv W_{v,1}\widehat{v}_1 + W_{v,2}\widehat{v}_2 = W_{v,1}\tilde{v} + W_{v,2}\int^* (\tilde{a} - \tilde{\omega} \times \tilde{v})\mathrm{d}t \quad (18)$$

where the sensory weights ($W_{a,1}$, $W_{a,2}$, $W_{v,1}$ and $W_{a,2}$) are between zero and one, and $\int^* dt$ designates a leaky integration with a time constant $\tau_a = 0.13$ s. The time constant τ_a has been chosen to fit reported human translational VOR responses (Busettini et al. 1994).

2.6 The gravito-inertial force resolution

Neither tonic nor phasic otolithic afferents distinguish gravity from linear acceleration (Anderson et al. 1978; Fernandez and Goldberg 1976a; Loe et al. 1973) since tonic and phasic afferents discharge similarly to changes in gravito-inertial force due to either tilt or translation. However, in our model the tonic (''regular'') afferent signals contribute preferentially to the estimate of gravity, and the phasic (''irregular'') afferent signals contribute preferentially to the estimate of linear acceleration, as previously suggested (Droulez and Darlot 1989; Mayne 1974; Young and Meiry 1968).

To compute the sensory estimates of gravity $\tilde{g}$ and linear acceleration $\tilde{a}$, the ''frequency completion mechanism'' in (8) has to be modified slightly. Indeed, to estimate gravity ($g = f + a$), the CNS needs to add the low-frequency content of an estimate of linear acceleration to the tonic otolithic afferent signal. Similarly, to estimate linear acceleration ($a = g - f$), the CNS needs to subtract the phasic otolithic afferent signal from the high-frequency content of an estimate of gravity.

Therefore, to compute the sensory estimate of gravity $\tilde{g}$, we hypothesize that the CNS adds to the tonic otolithic afferent signal the sensory estimate of linear acceleration $\tilde{a}$ filtered by an internal model of the tonic otolithic afferents $\hat{\mathbf{T}}_{ton} = \mathbf{T}_{ton}$:

$$\tilde{g} = \mathbf{T}_{ton}f + \hat{\mathbf{T}}_{ton}\tilde{a} + (\mathbf{I} - \hat{\mathbf{T}}_{ton})\hat{g} \quad (19)$$

Similarly, to compute the sensory estimate of linear acceleration $\tilde{a}$, we hypothesize that the CNS subtracts the phasic otolithic afferent signal from the central estimate of gravity $\hat{g}$ filtered by an internal model of the phasic otolithic afferents $\hat{\mathbf{T}}_{pha} = \mathbf{T}_{pha}$:

$$\tilde{a} = \mathbf{H}_a[-\mathbf{T}_{pha}f + \hat{\mathbf{T}}_{pha}\hat{g} + (\mathbf{I} - \hat{\mathbf{T}}_{pha})\hat{a}] \quad (20)$$

Since phasic units have a DC component (Appendix A), an additional filter $\mathbf{H}_a$ is added to the computing of the sensory estimate of linear acceleration $\tilde{a}$ to prevent any persistent non-zero estimates of linear acceleration ($\tilde{a}$ and $\hat{a}$) in the absence of movements. The diagonal elements of the transfer function $\mathbf{H}_a$ are first-order high-pass filters with a time constant $\tau_i = 200$ s. (The value of this time constant has little influence on simulated data

and has been arbitrarily chosen so that any estimates of linear acceleration are negligible after about 600 seconds with no head movement.)

2.7 Eye commands and the eye plant

One output of the sensory weighting model of visual–vestibular interactions is the slow-phase eye angular velocity in head e. To move the eye plant (Appendix A), a motor command e_M is computed by the CNS and sent to the motoneurons innervating the six extraocular muscles. The total eye command e_M is the sum of the compensatory reflexive eye command e_R and smooth pursuit command e_P. The total reflexive eye command e_R is the sum of the angular (e_A) and translational (e_T) reflexive commands. To simulate the fast-rise component of the optokinetic nystagmus (OKN), a 2D version of an existing smooth-pursuit model (Robinson et al. 1986) is implemented. (The mathematical descriptions of the motor commands and pursuit system are detailed in Appendix C.)

Table 1. Free parameters of the sensory weighting model

Parameter	Value
$W_{\omega,1}$	0.5
$W_{\omega,2}$	0.1
$W_{r,1}$	0.85
$W_{g,1}$	0.4
$W_{a,1}$	0.4
$W_{v,1}$	0.6
γ	0.7
τ_a	0.13 s
τ_i	200 s

2.8 Simulation

The sensory weighting model is implemented with the Matlab-Simulink software package (MathWorks Natick, Mass.) and a fourth-order variable-step Dormand–Prince algorithm is used for the simulations (the *ode45* function in Simulink). The model is defined by nine free parameters (seven sensory weights and two time constants) determined through a process of trial and error (Table 1); this single set of parameters is used for all simulations. To reduce from thirteen to seven the number of free parameters defining the various sensory weights, we assumed that the sum of weights equaled one ($\sum_{j=1}^{m} W_{i,j} = 1$) and used the following relationships (the values for $W_{\omega,3}$, $W_{r,2}$ and $W_{r,3}$ are discussed in Appendix C):

$$\begin{aligned} &W_{g,2} = 1 - W_{g,1}, W_{a,2} = 1 - W_{a,1}, W_{v,2} = 1 - W_{v,1}, \\ &W_{\omega,3} = 1 - W_{r,1} \\ &W_{r,2} = W_{\omega,1}\left(1 - W_{r,1}\right)/\left(W_{\omega,1} + W_{\omega,2}\right), \\ &W_{r,3} = W_{\omega,2}\left(1 - W_{r,1}\right)/\left(W_{\omega,1} + W_{\omega,2}\right) \end{aligned} \tag{21}$$

3 Results

3.1 Vision-canal interaction: Yaw rotation about an earth-vertical in darkness or in light

Results (Fig. 4) show that the model successfully simulates data from experiments investigating the angular VOR, OKN and optokinetic afternystagmus (OKAN), visual VOR (VVOR), and visual suppression. Switches S1, S2, and S3 are closed in the light (Fig. 3)

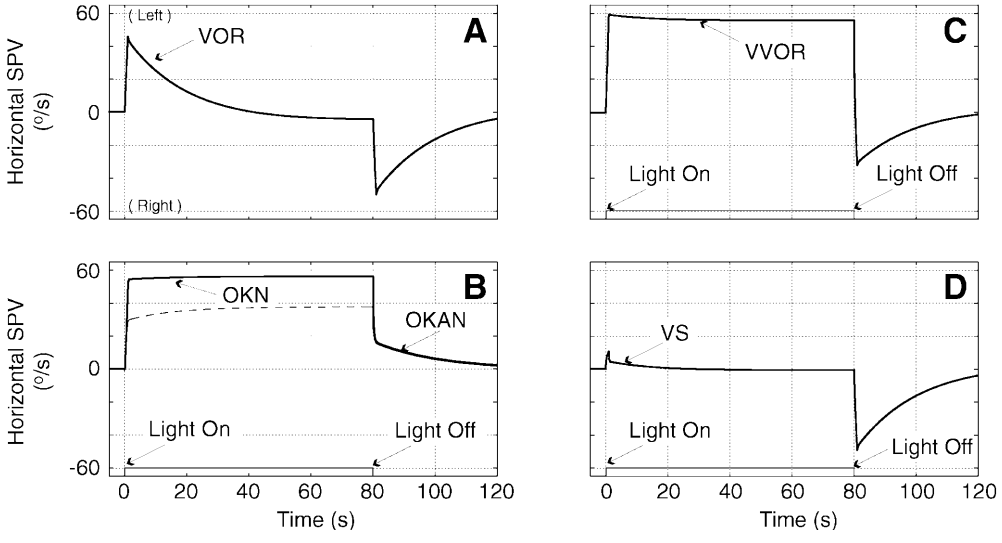

Fig. 4. Simulations of visual–vestibular interaction during yaw rotation about an earth-vertical axis. The subject is either immobile (**B**), or (**A, C, D**) rotates on-center about an earth-vertical axis in yaw at 60°/s to the subject's left (trapezoidal profile with an acceleration and a deceleration in 1 s and a constant velocity for 80 s). The subject is either in the dark (**A**), or the light is turned on at the beginning of the rotation and turned off after 80 s (**B, C, D**). (If there is a rotation movement, the rotation is stopped when the lights are turned off.) The different plots show the horizontal, slow-phase velocity (*SPV*) of the vestibulo-ocular reflex (*VOR*) (**A**), optokinetic nystagmus (*OKN*) and optokinetic afternystagmus (*OKAN*) with pursuit (*solid lines*) and without pursuit (*dashed lines*) (**B**), visual vestibulo-ocular reflex (VVOR) (**C**), and nystagmus during visual suppression (*VS*) (**D**)

and opened in darkness. In all protocols, the subject sits upright. Either the subject or an optokinetic drum, or both, are rotated in yaw about an earth-vertical axis.

In the first simulation (Fig. 4A), the subject is rotated in yaw to the right in the dark. Pre-rotatory VOR slow-phase eye velocity shows an exponential decay with a 46°/s peak, a dominant time constant of 20.8 s (see Appendix C) and a secondary time constant of 100 s. (The time constant values were determined by a least-square error fit to the sum of two exponential decays.) The dominant VOR time constant is greater that the canal afferent dominant time constant (6 s) and within the normal human VOR range (Barnes 1993). The post-rotatory nystagmus is a reversed version of the per-rotatory nystagmus.

In the second simulation (Fig. 4B), an optokinetic drum is rotated in yaw to the subject's left. During angular optokinetic stimulation with no movement of the head, the slow-phase eye velocity of the OKN has two distinct components: a fast-rise component driven by the pursuit system (80% of the OKN) and a slow-rise component (20% of the OKN) processed via interactions with the vestibular system (Cohen et al. 1981; Jell et al. 1984; Lafortune et al. 1986). After the lights are off, the early drop of post-rotatory slow-phase eye velocity from 56°/s to 18°/s ($t = 81$ s) is due to the inactivation of the pursuit system, but a small OKAN decay with a time constant of 20.8 s is still present as reported in humans (Cohen et al. 1981; Jell et al. 1984; Lafortune et al. 1986). (The time constant was determined by a least-square error fit to a single decaying exponential function).

In the third simulation (Fig. 4C), the subject is rotated in yaw to the right, while the optokinetic drum stays immobile in space. The resulting eye movements are referred to as the VVOR (Black et al. 1996). The steady-state VVOR pre-rotatory response has a compensatory gain of 0.93, which is consistent with experimental data. The initial peak results from the superimposition of vestibular and optokinetic responses. The post-rotatory response shows a reversal with a peak at −32°/s ($t = 81$ s), less than the peak of the post-rotatory VOR response in the dark (−50°/s in Fig. 4A). This reduced response is consistent with a superposition of the post-rotatory VOR response on the OKAN response, as shown experimentally (Cohen et al. 1981; Koenig et al. 1978).

In the fourth simulation (Fig. 4D), the subject and the optokinetic drum are rotated in yaw to the subject's left. Simulations show near total cancellation of the response (response smaller than 4°/s) after 3 s, in agreement with experimental results (Cohen et al. 1981; Koenig et al. 1978).

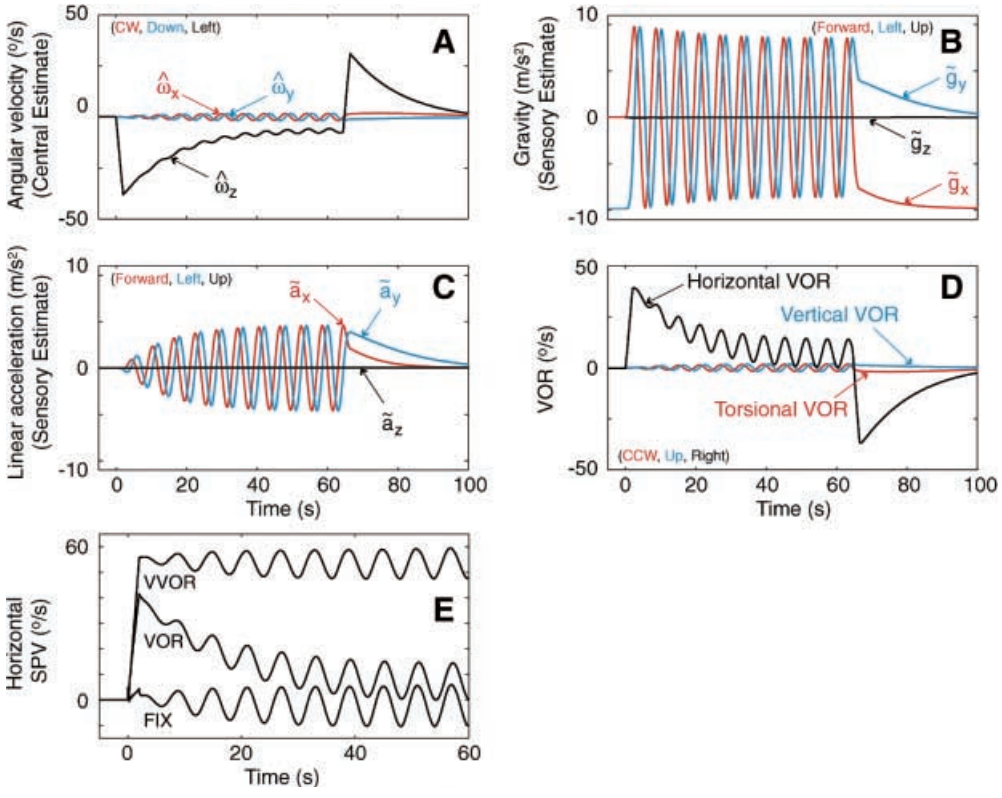

Fig. 5. Predicted responses induced by a 60°/s yaw rotation to the subject's right about an earth-horizontal axis ("barbecue-spit" rotation) in darkness and in lighted conditions (trapezoidal profile with acceleration and deceleration in 2 s). For a barbecue-spit rotation in darkness, modeling predictions of the per- and post-rotatory central estimate of head angular velocity $\hat{\omega}$ (**A**), sensory estimate of gravity $\tilde{g}$ (**B**), sensory estimate of linear acceleration $\tilde{a}$ (**C**), and total VOR (**D**). (After rotation, the subject is stopped in a nose-up orientation.) Also shown, modeling predictions of the per-rotatory reflexive horizontal slow-phase velocity SPV during a barbecue rotation in darkness (VOR), and in light with a space-fixed (VVOR) or head-fixed (FIX) visual surround (**E**). (For all plots, *red, blue*, and *black lines* represent the *x*-, *y*- and *z*-components, respectively. Direction conventions are indicated in *parentheses*.)

3.2 Canal-otolith-vision interaction: yaw rotation about an earth-horizontal axis (''barbecue protocol'')

In this simulation (Fig. 5), the subject is rotated in yaw for 60 s at 60°/s about an earth-horizontal axis, a so-called 90° off-vertical axis rotation or ''barbecue-spit'' rotation. Barbecue-spit rotations have been performed in humans (Benson and Bodin 1966b; Haslwanter et al. 2000; Wall and Furman 1990); while motion profiles were not identical, similar VOR characteristics were observed. In darkness, the horizontal VOR decays to a small non-zero compensatory bias, and a modulation is superimposed on the decaying horizontal VOR. Furthermore, non-compensatory sinusoidal vertical and torsional VOR components are present. In lighted conditions with a space-fixed visual surround the bias is larger than in darkness, and about equal to the stimulus angular velocity. With a head-fixed visual surround, there is no bias.

These experimental observations are accurately simulated by the sensory weighting model ($d = 0.9$ m in light and $d = 1.8$ m in darkness). The central estimate of horizontal head angular velocity decays to a non-zero compensatory bias (7°/s), and non-zero sinusoidal central estimates of vertical ($\hat{\omega}_y$, 4°/s peak-to-peak) and torsional ($\hat{\omega}_x$, 4°/s peak-to-peak) head angular velocity are elicited (Fig. 5A). As the horizontal semicircular canal cues decay, the sensory estimate of gravity $\tilde{g}$ keeps rotating at the same rate as the physical rotation but its magnitude decreases slightly (Fig. 5B). Since the sensory estimate of gravity $\tilde{g}$ lags behind the otolith measurement of gravity and its amplitude decays with time, a non-zero sensory estimate of linear acceleration $\tilde{a}$ is elicited (Fig. 5C). Therefore, a horizontal translational VOR component (15°/s peak-to-peak) superimposes on the total VOR (Fig. 5D, E).

During and after deceleration, the response is predominantly a horizontal VOR that decays and then reverses (Fig. 5D). Because of the ongoing canal rotation cue in the direction opposite the preceding motion (Fig. 5A), the sensory estimate of gravity $\tilde{g}$ is tilted away from the otolithic measurement of gravity (Fig. 5B). Because of this discrepancy between measured and estimated gravity, a non-zero interaural sensory estimate of linear acceleration ($\tilde{a}_y$) is elicited (Fig. 5C), leading to a horizontal translational VOR component that adds to the angular VOR component, as measured experimentally (Merfeld et al. 1999; Zupan et al. 2000). A small vertical eye movement (peak of ~2°/s) is also elicited (Fig. 5D), which slightly shifts the axis of eye rotation toward alignment with the sensory estimate of gravity $\tilde{g}$ rather than gravity. It takes about 40 s after stopping for the sensory estimate of gravity $\tilde{g}$ to realign with true gravity.

During a barbecue-spit rotation in light with a space-fixed visual surround, the sensory weighting model accurately simulates that the bias is large and nearly equal to the stimulus angular velocity (Fig. 5E). When the barbecue-spit rotation is simulated with a head-fixed visual surround, the sensory weighting model accurately simulates the absence of a bias (Fig. 5E).

3.3 Canal–otolith interaction: eccentric yaw rotation about an earth-vertical axis

During this simulation, the subject is rotated to the subject's right off-center in darkness. The subject sits upright at a radius of 0.514 m from the rotation axis and either faces the direction of motion (''facing motion'') or has his back toward the direction of motion (''back to motion''). This eccentric rotation results in a centrifugal force of 1 g that tilts the gravito-inertial force from 0° to 45° in roll as the angular velocity increases. The chair is then brought to a stop and the subject stays immobile for 60 s in darkness. Experimental data have shown differences in the eye movements between these two orientations in humans (Lansberg et al. 1965; Merfeld et al. 1992, 2001).

The model is able to reproduce the experimental differences observed in VOR eye movements between facing-motion and back-to-motion situations during the acceleration and steady-state phases (Merfeld et al. 2001). During the acceleration phase, the magnitude of the horizontal, slow-phase eye velocity is greater for the facing-motion orientation (161°/s, Fig. 6D) than for the back-to-motion orientation (119°/s, Fig. 6H). The vertical (15°/s peak) and torsional (15°/s peak) components reverse with the subject orientations (Fig. 6D). The central estimate of yaw angular velocity ($\hat{\omega}_z$) builds up in response to signals from the horizontal semicircular canals (Fig. 6A, E). As the gravito-inertial force builds up simultaneously, the central estimate of pitch angular velocity also builds up ($\hat{\omega}_y$), shifting the axis of the central estimate of angular velocity ($\hat{\omega}$) toward alignment with the gravito-inertial force. The direction of both central estimates of pitch ($\hat{\omega}_y$) and roll ($\hat{\omega}_x$) angular velocity reverse with the subject's orientation (Fig. 6A, E).

During acceleration, due to the horizontal canal cues the naso-occipital ($\tilde{g}_x$), interaural ($\tilde{g}_y$) and rostrocaudal ($\tilde{g}_z$) sensory estimates of gravity lag behind the gravito-inertial force (Fig. 6B, F). Consequently, a non-zero sensory estimate of linear acceleration $\tilde{a}$ is elicited, and non-zero central estimates of naso-occipital ($\hat{v}_x$), interaural ($\hat{v}_y$), and rostrocaudal ($\hat{v}_z$) linear velocity are thus calculated (Fig. 6C, G). The interaural central estimate of linear velocity ($\hat{v}_y$) peaks as the steady-state maximum centripetal acceleration is reached and decays thereafter to a plateau. The direction of the interaural central estimate of linear velocity ($\hat{v}_y$) reverses with the subject's orientation: rightward for ''facing-motion'' (Fig. 6C) and leftward for ''back to motion'' (Fig. 6G).

By definition, the angular VOR component compensates for the central estimate of angular velocity ($\hat{\omega}$). Due to the presence of a non-zero interaural central estimate of linear velocity ($\hat{v}_y$) that reverses with the subject's orientation, a horizontal translational VOR component (21°/s peak) is computed which adds to the horizontal angular VOR for ''facing-motion'' and subtracts for ''back to motion'' ($d = 1$ m is chosen for these simulations). This superimposition of the angular and linear components explains the difference in the peak and steady-state values of the horizontal VOR (Fig. 6D, H).

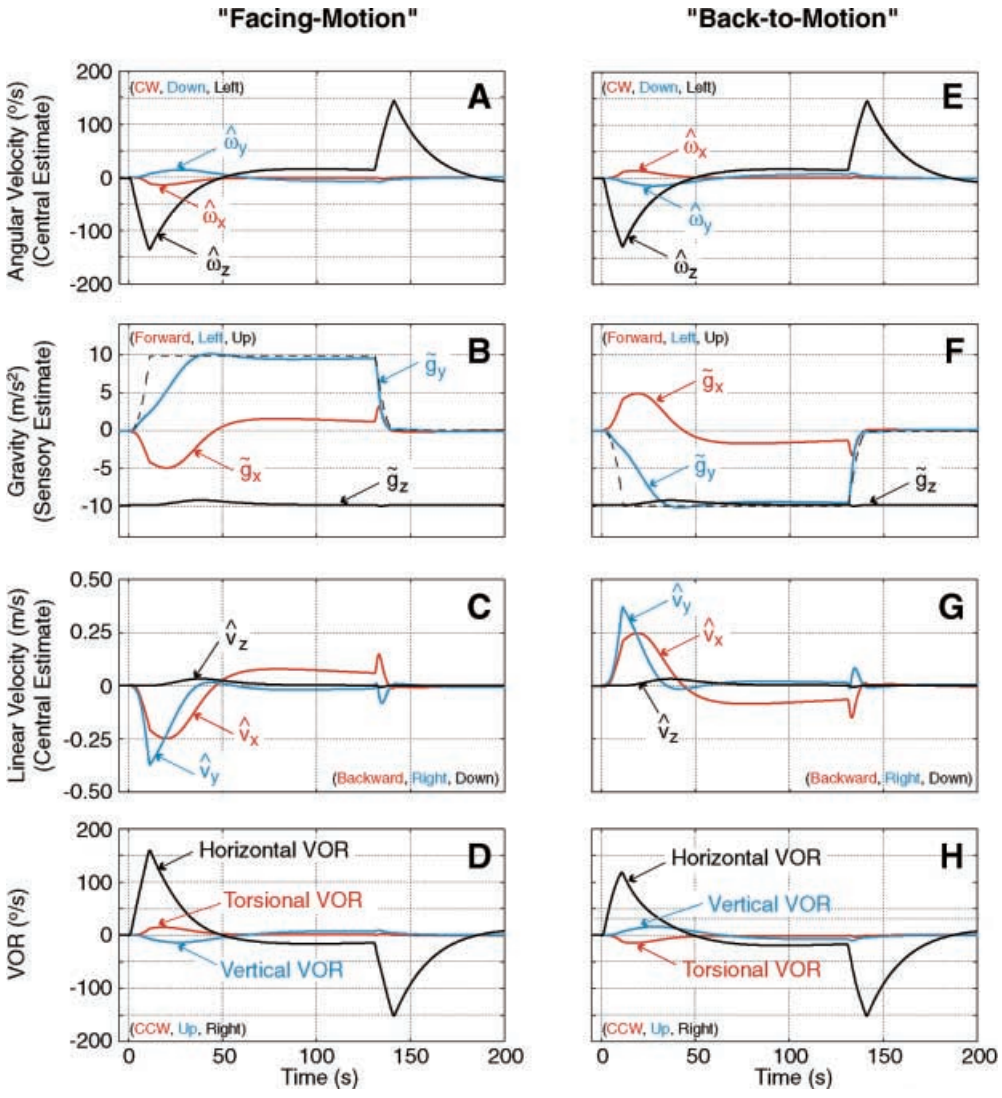

Fig. 6. Simulations of eccentric 250°/s yaw rotations to the subject's right (trapezoidal profile with acceleration and deceleration in 10 s and a constant velocity during 120 s). The *left column* shows the simulations with the subject facing the motion. The *right column* shows the simulations for a with the subject's back to the motion. Modeling predictions of the central estimate of head angular velocity $\hat{\omega}$ (**A, E**), sensory estimate of gravity $\tilde{g}$ (**B, F**) (the *dashed line* represents the physical interaural gravito-inertial force), central estimate of linear velocity $\hat{v}$ (**C, G**), and VOR responses (**D, H**) (For all plots, *red, blue* and *black lines* represent the *x*-, *y*- and *z*-components, respectively. Direction conventions are indicated in *parentheses*.)

Responses following deceleration are smaller–the primary response compensating for the post-rotatory central estimate of yaw angular velocity ($\hat{\omega}_z$) – since the translational VOR component is small and transient (peak 5°/s). In addition, the return of the interaural estimate for gravity ($\tilde{g}_y$) towards upright slightly leads the return of the gravito-inertial force as it has been reported (Merfeld et al. 2001).

4 Discussion

The model presented here allows accurate simulation of both eye movements and perceptions in response to a large variety of stimuli. The hypothesis that the CNS implements internal models of sensory dynamics, body dynamics, and physical relationships is the key to these successful simulations. As mentioned above an internal model is the neural implementation of physical principles that we describe with mathematical equations. The two principal questions in evaluating the sensory weighting approach are: (1) what are the physiological bases for the sensory weighting model? and (2) what is the originality of the sensory weighting model over previous approaches. These questions are addressed below.

4.1 Physiological bases of the sensory weighting model

4.1.1 Influence of rotational cues on the perception of self-orientation. The influence of rotational cues on human orientation is supported by various experimental observations. First, after a 90° post-rotatory tilt following a yaw rotation about an earth-vertical axis ("dumping"), subjects reported illusory tilt in a direction consistent

with the post-rotatory canal cue (Benson and Bodin 1966a; Merfeld et al. 1999; Von Holst and Grisebach 1951). During this paradigm, the duration of the post-rotatory sensation (Benson and Bodin 1966a) was not significantly influenced by head orientation, strengthening the hypothesis that the illusory tilt is canal driven. Similarly, others (Stockwell and Guedry 1970) have shown the influence of roll rotation cues from the semicircular canals on perceived roll tilt using actual dynamic roll tilts. In addition, during dumping protocols, VOR dynamics varied with head orientation (Benson and Bodin 1966a; Zupan et al. 2000). These variations were consistent with the hypothesis that canal cues were tilting the estimate of gravity away from measured gravity, eliciting a non-zero translational VOR in the absence of actual linear acceleration (Merfeld et al. 1999; Zupan et al. 2000). Using visual cues, Dichgans et al. (1972) also induced illusory tilts using roll vection. The direction of tilt reported was opposite to the direction of the optokinetic stimulus, consistent with the sensory weighting model simulated responses (data not shown).

In the sensory weighting model, we hypothesized that rotational cues influence the sensory estimate of gravity $\tilde{g}$ via the $\int \tilde{g} \times \tilde{\omega}\, dt$ component of the central estimate of gravity[5] $\hat{g}$ as shown in (10). This interaction between rotational and orientation cues leads to illusory tilt when either the head or the visual surround rotation axis is not collinear with gravity (Fig. 5A, B). During eccentric rotation, the presence of horizontal canal cues also influences the lag of the illusory roll tilt behind the tilt of the gravito-inertial force (Fig. 6B, F).

4.1.2 Influence of static otolithic cues on eye movements. Head orientation influences reflexive eye movements. In humans, after a post-rotatory tilt following a rotation about an earth-vertical axis (''dumping''), VOR responses have shorter time constants (Benson and Bodin 1966a; Fetter et al. 1992; Zupan et al. 2000) and the VOR rotation axis slightly shifts toward alignment with gravity (Fetter et al. 1996; Harris and Barnes 1987; Zupan et al. 2000). Similarly, eye movements in response to optokinetic stimuli about an axis not aligned with gravity also present an axis shift (Gizzi et al. 1994).

The sensory weighting model accurately simulates a shorter time constant of the angular VOR and a tendency of the VOR rotation axis to shift toward alignment with gravity after a post-rotatory tilt (data not shown, but similar to the post-rotatory responses following yaw rotation about an earth-horizontal axis in Fig. 5D). These simulated responses arise from interactions between rotational and orientation cues. More specifically, the second component $\langle \tilde{\omega}, \tilde{g}^{P} \rangle \tilde{g}$ of the intermediate estimate of head angular velocity $\bar{\omega}_2$ accounts for both the shortening of the eye movement time constant and the axis shift towards alignment with the sensory estimate of gravity. This component also accounts for an axis shift during optokinetic stimulation about an axis not aligned with gravity (data not shown), since vestibular and visual information share common pathways.

We can postulate that the processing of the intermediate estimate of head angular velocity $\bar{\omega}_2$ includes the uvulo-nodular cerebellar region, since a lesion of this region in rhesus and cynomolgus monkeys (Angelaki and Hess 1995; Wearne et al. 1996, 1998) suppresses the eye-movement characteristics (axis shift and time constant reduction) simulated by this component.

4.1.3 Influence of dynamic otolithic cues on eye movements. During yaw rotation about an off-vertical axis in darkness (e.g., about an earth-horizontal axis as in Fig. 5), the horizontal VOR exhibits a sinusoidal modulation with the same rate as the rotation, as well as a small usually compensatory bias in humans (Benson and Bodin 1966b; Darlot et al. 1988; Wall and Furman 1990). The compensatory bias arises from the utilization of otolith cues by the CNS, since a bias is still present after canal plugging (Cohen et al. 1983; Correia and Money 1970). In addition, vertical and torsional components are observed (Darlot et al. 1988; Harris and Barnes 1987; Haslwanter et al. 2000).

In the sensory weighting model, the horizontal sinusoidal modulation is primarily a translational VOR component compensatory for the estimated interaural linear acceleration. The compensatory bias arises from the utilization of the rotating otolith cues to calculate the intermediate estimate of head angular velocity $\bar{\omega}_2$. The first component $d\tilde{g}/dt \times \tilde{g}^{P}$ of the intermediate estimate of head angular velocity $\bar{\omega}_2$ accounts for the simulation of this compensatory bias. On the other hand, the second component $\langle \tilde{\omega}, \tilde{g}^{P} \rangle \tilde{g}$ of the intermediate estimate of head angular velocity $\bar{\omega}_2$ accounts for both vertical and torsional components that can be interpreted as the eye rotation axis shifting toward alignment with the sensory estimate of gravity $\tilde{g}$.

4.1.4 The gravito-inertial force resolution. Because of the mechanism used to separate the otolithic measurement of gravito-inertial force (f) into estimates of gravity ($\hat{g}$ and $\tilde{g}$) and linear acceleration ($\hat{a}$ and $\tilde{a}$), any discrepancy between the gravito-inertial force f and the central estimate of gravity $\hat{g}$ leads to a non-zero sensory estimate of linear acceleration $\tilde{a}$ according to (20), and therefore non-zero central estimates of linear acceleration $\hat{a}$ and velocity $\hat{v}$ according to (17) and (18). Therefore, when rotational cues induce an illusory tilt so that the central estimate of gravity $\hat{g}$ differs from measured gravity g, the sensory weighting model simulates non-zero sensory ($\tilde{a}$) and central ($\hat{a}$) estimates of linear acceleration, even in the absence of physical linear acceleration. This phenomenon is illustrated in Fig. 5B, and 5C during the post-rotatory period following a yaw rotation about an earth-horizontal axis. Various experimental data in humans support these simulated results. Indeed, these induced VOR responses have been observed in humans after a 90° post-rotatory tilt following a yaw rotation about an earth-vertical axis

[5] While the central estimate of gravity $\hat{g}$ is not accurate because of the integration in $\bar{g}_2 = \int \tilde{g} \times \tilde{\omega}\, dt$, it is important to notice that only its derivative or its high-pass filtered version through $\mathbf{H}_a.\mathbf{T}_{pha}$ (which are both accurate) are used to calculate the sensory estimates of gravity $\tilde{g}$ and linear acceleration $\tilde{a}$, respectively.

(Merfeld et al. 1999; Zupan et al. 2000), after a yaw rotation about an earth-horizontal axis (Zupan et al. 2000), after optokinetic yaw angular stimulation about an earth-horizontal axis (Wall et al. 1999), and after optokinetic roll angular stimulation about an earth-horizontal axis (Zupan et al. 2001).

4.1.5 The idiotropic vector. As suggested by Mittelstaedt (1983, 1986), the sensory weighting model implements an idiotropic vector $\tilde{g}^{M}$ in (13). The use of this idiotropic vector is indispensable to accurately simulate the sinusoidal variations of both vertical and torsional VOR during a yaw rotation about an earth-horizontal axis or "barbecue-spit" rotation (Fig. 5D), as shown by Haslwanter et al. (2000) with an alternative but similar approach. Because the idiotropic vector $\tilde{g}^{M}$ is used to calculate the second estimate of gravity $\tilde{g}^{P}$, the component $\langle \tilde{\omega}, \tilde{g}^{P} \rangle \tilde{g}$ of the intermediate estimate of head angular velocity $\hat{\omega}_2$ accounts for both vertical and torsional VOR during a barbecue-spit rotation.

Similarly, because the idiotropic vector $\tilde{g}^{M}$ is used to calculate the second estimate of gravity $\tilde{g}^{P}$in the component $\langle \tilde{\omega}, \tilde{g}^{P} \rangle \tilde{g}$ of the intermediate estimate of head angular velocity $\hat{\omega}_2$, the sensory weighting model can simulate a slight shift of the VOR rotation axis toward alignment with gravity after a 90° tilt following a yaw rotation about an earth-vertical axis ("dumping"), or after a yaw rotation about an earth-horizontal axis ("barbecue-spit" rotation) as observed in humans (Ferman et al. 1987; Fetter et al. 1996).

In addition, because the idiotropic vector $\tilde{g}^{M}$ is used to calculate the second estimate of gravity $\tilde{g}^{P}$, the orientation of $\tilde{g}^{P}$ accurately matches subjective orientation after roll tilt (Udo de Haes 1970). To make these simulations (data not shown), we weighted the otolith input with a gain of 1 for the x and y directions, and 0.8 for the z direction as suggested by Mittelstaedt (1983). (This change does not qualitatively affect any of the presented simulated responses.)

Since the orientation of $\tilde{g}^{P}$ matches so well the subjective orientation during eccentric rotation and after roll tilt, why not replace the sensory estimate of gravity $\tilde{g}$ by the second sensory estimate of gravity $\tilde{g}^{P}$ in (10) and (12)? Unfortunately, when we replaced the sensory estimate of gravity $\tilde{g}$ by $\tilde{g}^{P}$ in (10) and (12), we were not able to accurately simulate (data not shown) the influence of orientation on the optokinetic nystagmus (Gizzi et al. 1994). Indeed, when using $\tilde{g}$ in (10) and (12), we correctly simulate that the axis shift of the optokinetic nystagmus toward alignment with gravity is smaller for an earth-diagonal optokinetic stimulation with head upright than for a yaw optokinetic stimulation with head rolled 45°, as experimentally observed (Gizzi et al. 1994). When we replace the sensory estimate of gravity $\tilde{g}$ by $\tilde{g}^{P}$ in (10) and (12), we predicted the exact opposite result. One plausible explanation is that the CNS accesses $\tilde{g}^{P}$ at a perceptual level, while it accesses $\tilde{g}$ for reflexive oculomotor responses.

4.1.6 Significance of the sensory and central estimates. As seen in Sect. 3 as well as in the discussion above, it seems that the CNS may principally use central estimates $\hat{x}_i$ to elicit motor responses such as reflexive eye movements, and sensory estimates $\tilde{x}_i$ for perceptual responses. Indeed, the sensory weighting model accurately simulates VOR responses for a large variety of complex stimuli, and these VOR responses are compensatory to the central estimates of head angular velocity $\hat{\omega}$, eye angular velocity in space $\hat{r}$, and head linear velocity $\hat{v}$, as described in (C4) and (C11). Similarly, the second sensory estimate of gravity $\tilde{g}^{P}$ and the sensory estimate of linear acceleration $\tilde{a}$ accurately predict orientation and motion perception for a large variety of complex stimuli (see Sects. 3 and 4.1.5).

However, the difference between motor and perceptual responses cannot be sharply divided as resulting from differences between central and sensory estimates, respectively. Additional processing is essential, especially at the perceptual level. For example, perceptual responses during yaw rotation about a tilted axis (Darlot et al. 1987; Denise et al. 1988) or earth-horizontal axis (Guedry 1965) may result from additional low-pass and high-pass filtering of the sensory estimates of gravity and linear acceleration, respectively, as suggested by Mittelstaedt et al. (1989).

4.1.7 Parameter variations between species. While having similar horizontal dominant VOR time constants (~20 s), human and monkey VOR responses differ in many ways:

1. Larger bias in squirrel (Goldberg and Fernandez 1982) and cynomolgus monkeys (Cohen et al. 1983) during off-vertical axis rotation.
2. Larger shift of the VOR rotation axis toward alignment with gravity after a post-rotatory tilt in squirrel (Merfeld et al. 1993b) and rhesus or cynomolgus monkeys (Angelaki and Hess 1994; Wearne et al. 1998).
3. Larger shift of the VOR rotation axis toward alignment with gravity during eccentric rotation in squirrel (Merfeld and Young 1995) and rhesus or cynomolgus monkeys (Wearne et al. 1999).

To account for these differences between humans and monkeys, we adjusted two parameters:

1. The otolith contribution $\hat{\omega}_2$ to the central estimate of head angular velocity $\hat{\omega}$ is increased by increasing $W_{\omega,2}$ from 0.1 (human) to 0.53 (monkey).
2. To maintain the same horizontal dominant VOR time constant, the canal contribution $\tilde{\omega}$ to the central estimate of head angular velocity $\hat{\omega}$ is decreased by decreasing $W_{\omega,1}$ from 0.5 (human) to 0.07 (monkey), so that $\tau_{e,2} = 20.8$ s as described by (C6).

With these monkey parameters, the sensory weighting model simulates that the shift of the VOR rotation axis toward alignment with gravity is larger in monkeys than in humans following a yaw rotation about an off-vertical axis, as observed experimentally (Jaggi-Schwarz et al. 2000). Using the elements of the third column of $\mathbf{A}(\tilde{g}, \tilde{g}^{P})$ matrix described in (33) below, we predict a $\theta = 22°$ axis shift following a yaw rotation about an axis tilted 24°

with respect with earth-vertical, and a $\theta = 66^\circ$ axis shift following a yaw rotation about an earth-horizontal axis[6]. These results match previous experimental observations in rhesus monkeys that demonstrate a 16.7° and 68.6° average axis shift respectively (Figs. 6 and 7 in Jaggi-Schwarz et al. 2000). The same simulated responses hold after a 90° post-rotatory tilt following an earth-vertical axis yaw rotation, as observed experimentally in rhesus monkeys (Angelaki and Hess 1994).

Squirrel monkeys demonstrate a translational VOR during eccentric rotation (Merfeld and Young 1995) while cynomolgus monkeys do not (Wearne et al. 1999). This effect can be accounted for by keeping the canal contribution $\hat{g}_2$ to the central estimate of gravity $\hat{g}$ for squirrel monkeys the same as in humans ($W_{g,2} = 0.6$), while decreasing it in cynomolgus monkeys ($W_{g,2} = 0.2$).

4.1.8 Otolith afferent frequency segregation. In the sensory weighting model, the separation of gravito-inertial force into estimates of gravity and linear acceleration remains principally based on central interactions of otolith information with canal and visual information. The influence of canal information on tilt–translation segregation has been confirmed experimentally in rhesus monkeys, since the ability to distinguish tilt from translation was impaired by canal plugging (Angelaki et al. 1999). The implementations of tonic and phasic otolithic afferents in the sensory weighting model leads to better quantitative simulated responses than the observer model (Merfeld 1995a) which did not implement afferent segregation.

4.2 Originality of the Sensory Weighting model

4.2.1 Related modeling work. Early models of reflexive eye movements (Borah et al. 1988; Ormsby and Young 1977; Raphan et al. 1977; Robinson 1977; Schmid et al. 1979, 1980) were primarily aimed at describing the prolongation of both the vestibular nystagmus (compared to the activity of canal afferent) and the optokinetic nystagmus in darkness, referred to as OKAN. These models implemented sensory interactions between information coming from the semicircular canals and the visual system, and differed in their implementation of central pathways and non-linearity. None of these early models explicitly included internal models of sensory dynamics, body dynamics, or physical relationships.

Another early model of canal–otolith interactions focused on perceptual responses (Mayne 1974). Mayne's model implemented a peripheral frequency segregation between otolith afferents to separate tilt from translation as previously suggested by Young and Meiry (1968). The perception of vertical was also influenced by rotational cues in Mayne's model, and this implementation mimicking a physical relationship can be considered to be one of the earliest (though non-explicit) internal models used in a model of visual–vestibular interactions.

To account for the influence of otolithic information on visual–vestibular interactions, Robinson's (1977) original model, which also implemented a frequency completion mechanism, has been modified (Hain 1986). Hain's model implements one aspect of the influence of otolith information on rotational cues; i.e., the use of a rotating gravity vector measured by the otolith organs during off-vertical axis rotation to elicit a compensatory bias in the eye-movement response. But this model does not appear to predict later findings that the VOR rotation axis tends to shift toward alignment with gravity, or that canal cues influences the estimation of gravity. Finally, while sensory inputs are 3D, Hain's model focused primarily on horizontal eye movements.

Similarly, the velocity storage integrator model (Raphan and Sturm 1991; Raphan et al. 1977) has been modified to account for otolith influences on reflexive eye movements (Wearne et al. 1998, 1999). These recent models by Wearne et al. do not implement either the use of dynamic otolith information to estimate head rotation (e.g., it does not predict a compensatory bias in eye movements during off-vertical axis rotation) or the influence of semicircular canal cues on the estimation of gravity. These models do implement the tendency of the eye movement rotation axis to shift toward alignment with gravity.

Another model (Angelaki and Hess 1995) has mathematically described the influence of otolith inputs on monkeys reflexive eye movements. First, Angelaki and Hess hypothesize that vertical canal activity is *projected* onto the direction of gravity to account for the tendency of the eye pitch and roll rotation axis to align with gravity. Their transformation matrix is very similar to the one implemented in the sensory weighting model (33), but their model does not include either the influence of semicircular canal cues on the estimation of gravity or an idiotropic vector. In fact, their model assumed that a perfect neural representation of gravity existed since physical and neural representations were not distinguished. Second, to predict an axis shift from horizontal to either vertical or torsional components, the horizontal canal activity is *rotated* instead of *projected* onto the direction of gravity, as also described by Jaggi-Schwarz et al. (2000). These differences from the sensory weighting model may reflect differences in canal–otolith interactions between monkeys and humans.

More recently, canal–vision (Mergner et al. 1997) and canal–otolith (Mergner and Glasauer 1999) interactions have been modeled using an approach similar to the frequency completion mechanism described in (8) in the sensory weighting model, but without multicue averaging (7). In their model, the authors do not include an idiotropic vector and consider internal models of physical relationships that differ from those implemented in the sensory weighting model. For example, the estimate of head angular velocity elicited from otolith input is computed as $\hat{\omega}_2 = \mathrm{d}\tilde{g}/\mathrm{d}t \times \tilde{g}$ in (Mergner and Glasauer 1999) instead of $\hat{\omega}_2 = \mathrm{d}\tilde{g}/\mathrm{d}t \times \tilde{g}^{\mathrm{P}} + \langle \tilde{\omega}, \tilde{g}^{\mathrm{P}} \rangle \tilde{g}$ in the sensory weighting model. Because of the missing $\langle \tilde{\omega}, \tilde{g}^{\mathrm{P}} \rangle \tilde{g}$ component, Mergner's and Glasauer's (1999) model does not predict any vertical or torsional VOR

[6] We use $\theta = \tan^{-1}\left[W_{\omega,2}\hat{g}_{3,z}\sqrt{\tilde{g}_x^2 + \tilde{g}_y^2} \;/\left(W_{\omega,1} + W_{\omega,2}\hat{g}_{3,z}\tilde{g}_z\right)\right]$ with $\tilde{g} = g$ as a first approximation.

during yaw rotation about an earth-horizontal axis (Fig. 5D), or any vertical VOR during yaw eccentric rotation (Fig. 6D, H).

4.2.2 The velocity storage integrator model. The sensory weighting model formulates how the matrix $\mathbf{A}(\tilde{g},\tilde{g}^{\mathrm{P}})$ defining the velocity storage mechanism varies with head orientation as shown in (D2–D4), augmenting the empirical formulations of earlier studies (Dai et al. 1991; Gizzi et al. 1994; Raphan and Sturm 1991). If the idiotropic vector $\tilde{g}^{\mathrm{M}} = [0, 0, -1]$ replaces the vector $\tilde{g}^{\mathrm{P}}$, the matrix $\mathbf{A}(\tilde{g},\tilde{g}^{\mathrm{M}})$ detailed in (D6) is structurally identical to the velocity storage matrix proposed by Raphan and Sturm (1991).

For both canal and visual angular stimulation, the two non-diagonal elements in the last column of $\mathbf{A}(\tilde{g},\tilde{g}^{\mathrm{P}})$ and $\mathbf{A}(\tilde{g},\tilde{g}^{\mathrm{M}})$ are responsible for the cross-coupling from horizontal to vertical eye movements during roll tilt ($\tilde{g}_x = 0$), and from horizontal to torsional eye movements during pitch tilt ($\tilde{g}_y = 0$). This cross-coupling illustrates the tendency of the eye rotation axis to shift toward alignment with the sensory estimate of gravity $\tilde{g}$, as observed experimentally in humans for canal (Fetter et al. 1996; Zupan et al. 2000) and visual (Gizzi et al. 1994) stimulation.

The sensory weighting model includes two additional cross-coupling elements that are not included in the matrix used by Raphan and Sturm (1991): (1) a pitch-to-yaw cross-coupling element $W_{\omega,2}\tilde{g}_y^{\mathrm{P}}\tilde{g}_z$ during roll tilts, and (2) a roll-to-yaw cross-coupling element $W_{\omega,2}\tilde{g}_x^{\mathrm{P}}\tilde{g}_z$ during pitch tilts. These two additional cross-coupling elements permit the simulation of axis shifts following both roll and pitch rotations about an earth-vertical axis in agreement with the characteristics of monkey eye movements after post-rotatory tilts following a constant-velocity rotation (Angelaki and Hess 1994; Merfeld et al. 1993b).

4.2.3 The Observer models. The observer models are based on the hypothesis that the CNS includes internal models of sensory dynamics, body dynamics, and physical relationships (Glasauer 1992, 1993; Glasauer and Merfeld 1997; Merfeld 1995a, b; Merfeld et al. 1993a; Oman 1982). Another recent model (Angelaki et al. 1999) uses identical canal–otolith processing to predict the tilt–translation discrimination.

Although very close to the sensory weighting model, observer models differ in: (1) their use of internal loops, (2) their implementation of the gravito-inertial force resolution mechanism, (3) the absence of the implementation of an idiotropic vector, and (4) their complexity.

In the sensory weighting model, each internal feedback loop described by (7) and (8) is defined by a weight $W_{i,j}$. In the absence of noise, ideally accurate estimates are obtained for $\sum_{j=1}^{m} W_{i,j} = 1$ if $\hat{\mathbf{T}}_i = \mathbf{T}_i$. In Merfeld's Observer models (Merfeld 1995a, b; Merfeld et al. 1993a), each feedback loop is defined by a gain $k_{i,j}$ (which do not add to unity). If we neglect the internal model of physical relationships that transforms sensory estimates to intermediate estimates ($\bar{x}_{i,j} = \tilde{x}_i = \hat{x}_i$), the simple relationship $k_{i,j} = W_{i,j}/\left(1 - \sum_{j=1}^{m} W_{i,j}\right)$ would link gains and weights if both models were equivalent. Therefore, perfect estimates for the sensory weighting model in the absence of noise would require infinite gains in Merfeld's observer model. Similarly, in observer models with a Kalman filter approach (Glasauer 1992, 1993), feedback loops are defined by a gain $k_{i,j}$ followed by an additional integration: this integration stems from the formulation of the system model since Gaussian noise is assumed to account for the uncertainties in the model regarding the variable to be estimated. The additional integration term also lead to differences in optimal estimates compared to the sensory weighting model and Merfeld's observer model.

Second, the sensory weighting model implements a gravito-inertial force resolution mechanism where the estimate of gravity is not constrained to have a constant norm. Merfeld's model (Merfeld 1995b; Merfeld et al. 1995) constrained the internal estimate of gravity to a constant norm, while Glasauer's (1992, 1993) model did not. This difference does not substantially change the simulated responses except during centrifugation experiments, as previously discussed (Merfeld 1995b; Merfeld and Young 1995).

Third, the sensory weighting model includes an idiotropic vector while Merfeld's most recent observer model (Merfeld 1995a) does not. Glasauer's (1992, 1993) model did include an idiotropic vector, although in a different place from that in the sensory weighting model. Therefore, Merfeld's model does not for example, predict sinusoidal vertical and torsional components during yaw rotation about an earth-horizontal axis. However, these components are accurately predicted by a more recent implementation of the observer model (Haslwanter et al. 2000) that includes an idiotropic-like component.

Fourth, the sensory weighting model implements visual–vestibular interactions while Merfeld's (1995a) observer model implements vestibular-only interactions.

4.2.4 The coherence constraint model. The "coherence constraint" models (Darlot 1993; Darlot et al. 1996; Denise and Darlot 1993; Droulez and Darlot 1989; Zupan 1995; Zupan et al. 1994) are also based on the concept of internal models of sensory dynamics, body dynamics, and physical relationships.

Although originally inspired by the coherence constraint model, the sensory weighting model rejects the notion of captor specificity, merging towards the observer approach. In the coherence constraint model, the reflexive eye movements are compensatory to the sensory estimates of physical variables that principally depend on the sensory signal issued from a "dedicated" sensor as described by (9) and (12). In contrast, the sensory weighting model uses central estimates of physical variables to compute the compensatory reflexive eye movements. By definition, all available sensory information is used to compute a central estimate in a proportion defined by a sensory weight as described in (7), and no sensor is considered "dedicated" to a certain central estimate.

Second, the coherence constraint and sensory weighting models implement different gravito-inertial force resolution mechanisms. Indeed, the coherence constraint model adds $\hat{\mathbf{T}}_{\text{ton}}\hat{\boldsymbol{a}}$ to $\mathbf{T}_{\text{ton}}f$ in (19) and subtracts $\mathbf{T}_{\text{pha}}f$ from $\hat{\mathbf{T}}_{\text{pha}}\tilde{\boldsymbol{g}}$ in (20) to estimate gravity and linear acceleration, while the sensory weighting model adds $\hat{\mathbf{T}}_{\text{ton}}\tilde{\boldsymbol{a}}$ to $\mathbf{T}_{\text{ton}}f$ in (19) and subtracts $\mathbf{T}_{\text{pha}}f$ from $\hat{\mathbf{T}}_{\text{pha}}\hat{\boldsymbol{g}}$ in (20). Because of these different choices, a previous version of the sensory weighting model was able to accurately predict motion sickness occurrence during off-vertical axis rotation (Zupan 1995; Zupan et al. 1994), while simulated responses by the original coherence constraint model (Droulez and Darlot 1989) were not as accurate.

Third, the coherence constraint model does not implement an idiotropic vector and uses $\tilde{\boldsymbol{g}}$ instead of $\tilde{\boldsymbol{g}}^{\text{P}}$ in (12) to predict the intermediate estimate of head angular velocity $\widehat{\omega}_2$. Because of this choice, the coherence constraint model cannot predict the shift of the VOR rotation axis toward alignment with gravity when the rotational cues are perpendicular to gravity, as observed experimentally after a 90° post-rotatory tilt following a yaw earth-vertical axis rotation or during a yaw rotation about an earth-horizontal axis.

5 Conclusion

The sensory weighting model is a general model of sensory integration that has been successfully applied to model canal–vision, canal–otolith, vision–otolith, and idiotropic interactions and associated eye movements. The only requirements of the sensory weighting model are the identification of the sensors involved, their dynamic characteristics, and the physical relationships linking the various measured variables. This model of visual–vestibular interactions successfully simulated reflexive eye movements as well as motion and orientation perception in response to a large variety of 3D stimuli in darkness and in lighted conditions. This model has been used to design experiments (Merfeld et al. 1999; Zupan et al. 2000), since it provides insight into the neural processes underlying sensory integration.

Acknowledgements. We thank both reviewers for their thoughtful comments that greatly improved this manuscript. We also thank G. McCollum, R.J. Peterka, S. Oster, R. Lewis, and I. Israel for their advice on the writing of this paper. This work was supported by the ESA External Fellowship Program, and NIDCD grants DC03065 and DC04644. Preliminary findings were presented in a PhD thesis (Zupan 1995) supported by DRET grant 91/1291A/DRET, CNES grant 93/CNES/0255, and the Ecole Nationale Supérieure des Télécommunications. Upon request, the authors will be happy to provide *Simulink* and *Matlab* files to implement and simulate the sensory weighting model.

Appendix A: Sensory and body dynamics

A.1 Semicircular canal

The head angular velocity ω is measured by the semicircular canals in a head-fixed frame of reference. The three semicircular canals are assumed to be mutually orthogonal and aligned respectively with the head *x*-, *y*-, and *z*-axes[7]. They are modeled by a diagonal transfer function matrix $\mathbf{T}_{\text{scc}}$, the diagonal elements of which are equal to

$$s^2\tau_{\omega,0}\tau_{\omega,1}/\left[(1+s\tau_{\omega,0})(1+s\tau_{\omega,1})\right] \tag{A1}$$

where $\tau_{\omega,0} = 6$ s and $\tau_{\omega,1} = 100$ s are the dominant and adaptation time constants, respectively (Fernandez and Goldberg 1971). For simplicity and to show that the internal model does not have to perfectly match the sensor dynamics to accurately predict experimental results, the internal model of the semicircular canal dynamics is modeled by a diagonal transfer function matrix $\hat{\mathbf{T}}_{\text{scc}}$ the diagonal elements of which are equal to

$$s\tau_{\omega,0}/(1+s\tau_{\omega,0}) \tag{A2}$$

A.2 Otolith organs

The otolithic primary afferents in monkeys can be segregated into tonic ("regular") and phasic ("irregular") afferents (Fernandez and Goldberg 1976b). The pool of tonic otolith afferents is modeled by a diagonal transfer function matrix $\mathbf{T}_{\text{ton}}$, the diagonal elements of which are equal to

$$1/(1+s\tau_{\text{oto}}) \tag{A3}$$

where $\tau_{\text{oto}} = 0.03$ s. The internal model $\hat{\mathbf{T}}_{\text{ton}}$ is chosen so that $\hat{\mathbf{T}}_{\text{ton}} = \mathbf{T}_{\text{ton}}$.

The pool of otolithic phasic afferents is modeled by a diagonal transfer function matrix $\mathbf{T}_{\text{pha}}$, the diagonal elements of which are equal to

$$\tau_{\text{a},0}\left(1+s\tau_{\text{a},1}\right)/\left[\tau_{\text{a},1}(1+s\tau_{\text{a},0})(1+s\tau_{\text{oto}})\right] \tag{A4}$$

where $\tau_{\text{oto}} = 0.001$ s, $\tau_{\text{a},0} = 0.55$ s, and $\tau_{\text{a},1} = 160$ s. The smaller time constant $\tau_{\text{oto}} = 0.001$ s common to both tonic and phasic units (Fernandez and Goldberg 1976b) may reflect the mechanics of otolith motion. The internal model $\hat{\mathbf{T}}_{pha}$is chosen so that $\hat{\mathbf{T}}_{\text{pha}} = \mathbf{T}_{\text{pha}}$.

A.3 Angular information in the visual system

The present work does not deal with the visual processing that separates the optic flow into self-motion and movement of the visual surround (Droulez and Cornilleau-Pérès 1993; Simpson 1984). The angular and linear components of any visual movement are assumed

[7] The true orientations of the anterior and posterior canal are approximately rotated 45° and 135°, respectively, from the forward direction that is orthogonal to the horizontal canal axis (Curthoys et al. 1977). Anatomical accuracy can be implemented by replacing the transfer function T(*s*) with one representing the geometry of the semicircular canals. If the same changes are made in the internal model T(*s*), the model-simulated responses will remain completely unchanged since this is equivalent to a simple coordinate transformation.

to be available as separate stimuli measured by the visual system, using retinal slip and image deformation.

The part of the visual system that extracts angular information from retinal slip is modeled by a 3D transfer function matrix $\mathbf{T}_{rs}$, the diagonal elements of which are equal to

$$1/(1+s\tau_r) \tag{A5}$$

where $\tau_r = 0.15$ s. This time constant has been chosen to fit eye movements in response to visual surround rotation (Cohen et al. 1981; Jell et al. 1984).

The part of the visual system that extracts linear information from image deformation is modeled by a diagonal transfer function matrix $\mathbf{T}_{id}$, the diagonal elements of which are equal to

$$1/(1+s\tau_v) \tag{A6}$$

where $\tau_v = 0.15$ s. This time constant has been chosen to fit eye movements during translation of the visual surround (Busettini et al. 1994). The internal model $\hat{\mathbf{T}}_{id}$ is chosen so that $\hat{\mathbf{T}}_{id} = \mathbf{T}_{id}$.

A.4 Eye plant

The dynamics of the eye plant are modeled by a diagonal transfer function matrix $\mathbf{T}_{eye}$, the diagonal elements of which are equal to

$$1/(1+s\tau_{e,1}) \tag{A7}$$

where $\tau_{e,1} = 0.003$ s is the smallest time constant characterizing the eye plant (Fuchs et al. 1988) since the other time constants are supposed to be cancelled by a "neural integrator" (Minor and Goldberg 1991). This eye-plant time constant corresponds to a ~50-Hz cutoff frequency, in agreement with VOR characteristics during high-frequency sinusoidal rotations up to 15 Hz in squirrel monkey (Robinson et al. 1986). The internal model $\hat{\mathbf{T}}_{eye}$ is chosen so that $\hat{\mathbf{T}}_{eye} = \mathbf{T}_{eye}$. By definition, the eye angular velocity in head e and the motor command e_M sent to the motoneurons innervating the extra-ocular eye muscles are linked by the relation

$$e = \mathbf{T}_{eye} e_M \tag{A8}$$

Appendix B: one physical variable and two sensors

Using (5) and (6), the sensory estimate $\tilde{x}_1$ and central estimate $\hat{x}_1$ can be computed as

$$\begin{aligned}\tilde{x}_1 \equiv \hat{x}_{1,1} &= \mathbf{T}_1 x_1 + \hat{x}_1 - \hat{\mathbf{T}}_1 \hat{x}_1 \\ &= \frac{\mathbf{I}}{\mathbf{I} - W_{1,1}(\mathbf{I} - \hat{\mathbf{T}}_1)} \left[\mathbf{T}_1 x_1 + W_{1,2}(\mathbf{I} - \hat{\mathbf{T}}_1)\hat{x}_{1,2}\right]\end{aligned} \tag{B1}$$

$$\hat{x}_1 = \frac{\mathbf{I}}{\mathbf{I} - W_{1,1}(\mathbf{I} - \hat{\mathbf{T}}_1)} \left(W_{1,1}\mathbf{T}_1 x_1 + W_{1,2}\hat{x}_{1,2}\right) \tag{B2}$$

In the sensory weighting model, head angular velocity and linear acceleration are primarily estimated from high-pass-filtered sensory signals. If corresponding sensory dynamics are modeled by a first-order high-pass filter $\mathbf{T}_1 = \tau s/(1+\tau s)\cdot\mathbf{I}$ with $\hat{\mathbf{T}}_1 = \mathbf{T}_1$, the sensory estimate $\tilde{\mathbf{x}}_1$ is composed of the high-pass-filtered version of x_1 (gain 1) with a time constant increased by a factor of $1/(1-W_{1,1})$, and the low-pass-filtered second estimate $\hat{x}_{1,2}$ which achieves frequency completion. The gain of the low-pass-filtered version of $\hat{x}_{1,2}$ is $W_{1,2}/(1-W_{1,1})$; therefore, for a gain of 1, $W_{1,2} = 1 - W_{1,1}$ or $W_{1,1} + W_{1,2} = 1$. Similarly, the central estimate $\hat{x}_1$ is in the high-frequency range composed of a weighted average of high-pass-filtered signal x_1 (gain $W_{1,1}$) and intermediate estimates $\hat{x}_{1,2}$ (gain $W_{1,2}$), whereas it is equal to the sensory estimate in the low-frequency range.

In the sensory weighting model, gravity, linear velocity, and eye angular velocity in space are primarily estimated from low-pass-filtered sensory signals. If corresponding sensory dynamics are modeled by a first-order low-pass-filter $\mathbf{T}_1 = 1/(1+\tau s)\cdot\mathbf{I}$ with $\hat{\mathbf{T}}_1 = \mathbf{T}_1$, the complementary filter $\mathbf{I} - \hat{\mathbf{T}}_1$ is a high-pass filter and the corresponding feedback loop is an algebraic loop, thus requiring a small manipulation. We chose to break the algebraic loop with a low-pass filter of the form $1/(1+\varepsilon s)\mathbf{I}$, with $\varepsilon = 1$ ms. This transfer function has a cutoff frequency of 160 Hz, so it breaks the algebraic loop with little or no dynamic influence on the simulated responses. In this case, the sensory estimate $\tilde{x}_1$ is composed of the low-pass-filtered version of x_1 (gain 1) with a time constant decreased by a factor of $(1-W_{1,1})$, and the high-pass-filtered second estimate $\hat{x}_{1,2}$ which achieves frequency completion. The gain of the high-pass-filtered version of $\hat{x}_{1,2}$ is $W_{1,2}/(1-W_{1,1})$. Similarly, the central estimate $\hat{x}_1$ is in the low-frequency range composed of a weighted average of low-pass-filtered signal x_1 (gain $W_{1,2}$) and intermediate estimates $\hat{x}_{1,2}$ (gain $W_{1,2}$), whereas it is equal to the sensory estimate in the high-frequency range.

Finally, in the presence of noise n in the sensory signal, the noise in the sensory estimate is only augmented by either a low- or high-frequency part of the sensory neural noise n.

Appendix C: Eye command and eye movements

C.1 The total eye command and eye movements

The total eye command sent to the motoneurons innervating the eye muscles is the sum of reflexive (e_R) and smooth pursuit (e_P) eye commands:

$$e_M = e_R + e_P \tag{C1}$$

Both commands e_R and e_P lead to eye rotation. The motor command efference copy $\hat{e}_M$ is assumed to match the motor command ($\hat{e}_M = e_M$). The sensory estimate of eye angular velocity in head $\tilde{e}$ is obtained from the efference copy $\hat{e}_M$ as follows:

$$\tilde{e} = \hat{\mathbf{T}}_{\text{eye}}\hat{e}_{\text{M}} \tag{C2}$$

C.2 The compensatory reflexive eye movements

The reflexive eye command e_{R} is the sum of angular (e_{A}) and translational (e_{T}) reflexive eye commands:

$$e_{\text{R}} = e_{\text{A}} + e_{\text{T}} \tag{C3}$$

C.2.1 The angular reflexive eye movements. The angular reflexive eye command e_{A} compensates for head angular movements (angular VOR) and for angular displacements of the visual surround (OKN and OKAN). This command is computed using central estimates of head angular velocity $\hat{\omega}$ and eye angular velocity in space $\hat{r}$:

$$e_{\text{A}} = -\hat{\omega} - \hat{r} \tag{C4}$$

During a rotation about an earth-vertical axis, the angular motor command e_{A} and efference copy of this motor command $\hat{e}_{\text{M}}$ are equal, and the intermediate estimate of head angular velocity $\bar{\omega}_2$ is equal to the sensory estimate of head angular velocity $\tilde{\omega}$ according to (12). To determine the dominant VOR time constant during rotation about an earth-vertical axis, we combine (A8), (C2) and (C4) with (15), (16), and (5) expressed for both sensory estimates of head angular velocity $\tilde{\omega}$ and eye angular in space $\tilde{r}$. To be able to describe explicitly the VOR dynamics, we neglected the eye-plant transfer function $\mathbf{T}_{\text{eye}}$, its internal model $\hat{\mathbf{T}}_{\text{eye}}$, and any "anti-algebraic loop" filters $1/(1+\varepsilon s)\mathbf{I}$, since their time constants are at least one order of magnitude smaller than the dominant VOR time constant (~ 20 s):

$$\begin{aligned} e &= -\mathbf{T}_{\text{VOR}}\omega \text{ with } \mathbf{T}_{\text{VOR}}(s) \\ &\approx \frac{s^2\left(1/\tau_{\text{e},0}+s\right)}{\left(1/\tau_{\text{e},1}+s\right)\left(1/\tau_{\text{e},2}+s\right)\left(1/\tau_{\text{e},3}+s\right)}\, G_{\text{VOR}}\mathbf{I} \end{aligned} \tag{C5}$$

Introducing the parameters $W_{\text{e}} = 1 + W_{\omega,1} + W_{\omega,2} - W_{\text{r},1}$ and $\kappa = 2\left(1-W_{\text{r},1}\right)\left(1-W_{\text{e}}\right)\tau_{\text{r}}/\tau_{\omega,0}$, the zero and poles of $\mathbf{T}_{\text{VOR}}(s)$ are equal to

$$\begin{aligned} &\tau_{\text{e},0} = \tau_{\text{r},1}(1-W_{\text{r},1})(1+W_{\text{e}})/W_{\text{e}} = 0.05 \text{ s}, \\ &\tau_{\text{e},1} = \frac{4\left(1-W_{\text{r},1}\right)\tau_{\text{r}}}{1+\kappa+\sqrt{(1-\kappa)^2-4\left(1-W_{\text{r},1}\right)\kappa}} = 0.045\,\text{s}, \\ &\tau_{\text{e},2} = \frac{4\left(1-W_{\text{r},1}\right)\tau_{\text{r}}}{1+\kappa-\sqrt{(1-\kappa)^2-4\left(1-W_{\text{r},1}\right)\kappa}} = 20.9 \text{ s}, \\ &\text{and } \tau_{\text{e},3} = \tau_{\omega,1} = 100\,\text{s} \end{aligned} \tag{C6}$$

One can notice the quasi-cancellation of the zero $\tau_{\text{e},0}$ by the pole $\tau_{\text{e},1}$, and the lengthening of the dominant VOR time constant $\tau_{\text{e},2} = 20.9$ s when compared to the dominant canal time constant $\tau_{\omega,0} = 6$ s (the approximations are legitimate since least-square error fits demonstrated that $\tau_{\text{e},2} = 20.9$ s and $\tau_{\text{e},3} = 100$ s in Sect. 3). Different weights $W_{\omega,1}$, $W_{\omega,2}$, and $W_{\text{r},1}$ for the yaw, pitch, and roll components of the intermediate estimates of head angular velocity would lead to different horizontal, vertical, and torsional VOR time constants, as observed experimentally (Melvill Jones et al. 1964).

To minimize the number of free parameters, the relative contribution of $\tilde{e}$ in both central estimates of head angular velocity $\hat{\omega}$ and eye angular velocity $\hat{r}$ is considered to be the same:

$$W_{\omega,3} = W_{\text{r},2} + W_{\text{r},3} \tag{C7}$$

The relative contribution of canal and otolith information in the central estimates of head angular velocity $\hat{\omega}$ and eye angular velocity $\hat{r}$ is also considered to be the same:

$$W_{\omega,1}/W_{\omega,2} = W_{\text{r},2}/W_{\text{r},3} \tag{C8}$$

Using (C7) and (C8), knowing that $W_{\omega,1} + W_{\omega,2} + W_{\omega,3} = 1$ and $W_{\text{r},1} + W_{\text{r},2} + W_{\text{r},3} = 1$, we obtain

$$W_{\text{r},2} = W_{\omega,1}\left(1-W_{\text{r},1}\right)/\left(W_{\omega,1}+W_{\omega,2}\right) \tag{C9}$$

$$W_{\text{r},3} = W_{\omega,2}\left(1-W_{\text{r},1}\right)/\left(W_{\omega,1}+W_{\omega,2}\right) \tag{C10}$$

C.2.2 The translational reflexive eye movements. The translational reflexive eye command e_{T} compensates for head translation and translation of the visual surround. This command depends on target distance and target orientation (Paige 1989; Paige and Tomko 1991; Schwarz and Miles 1991; Schwarz et al. 1989; Tomko and Paige 1992), and is computed using the central estimate of linear velocity $\hat{v}$ with a simple cross-product (Viirre et al. 1986):

$$e_{\text{T}} = -\hat{p} \times \hat{v} \tag{C11}$$

where $\hat{p}$ is a vector aligned with the estimated gaze direction ($\hat{p}$ is collinear with $i = [1,0,0]$ for gaze straight-ahead) and its norm is the inverse of the estimated distance d from the eye to the target). For simulation in darkness, $\hat{p} = i/d$, with d equal to the distance of a fixed imaginary target.

C.3 The pursuit system

In the smooth pursuit model of Robinson et al. (1986), the input to the CNS is a 1D "reconstructed target velocity" $\dot{T}'$:

$$\dot{T}'(s) = \dot{E}'(s)/(1+sT_{\text{e}2}) - \dot{e}(s) \tag{C12}$$

where $\dot{E}'$ is the efference copy of the eye command, $\dot{e}$ is the retinal slip, and $T_{\text{e}2}$ is the time constant characterizing the eye plant dynamics. (For simplicity, we neglected the three "pure delays" of 30 ms, 50 ms, and 80 ms.) An implicit "neural integrator" cancels the dominant time constant ($T_{e1} = 224$ ms) suppress.

In the sensory weighting model, we implement a 2D version of Robinson's model for horizontal and vertical smooth pursuit. The horizontal and vertical pursuit systems are considered independent. To account for passive head movements, we replaced the "reconstructed target velocity" with the central estimate of target velocity $\hat{t}$:

$$\hat{t} = \Pi_{yz}(\hat{\omega} + \tilde{e} - \mathbf{T}_{\mathrm{rs}} r_{\mathrm{e}}) \tag{C13}$$

where $\hat{\omega}$ is the central estimate of head angular velocity, $\tilde{e}$ is the sensory estimate of eye angular velocity in head, r_{e} is the opposite of the retinal slip, $\mathbf{T}_{\mathrm{rs}}$ is the transfer function of the visual system processing retinal slip, and Π_{yz} is the projection of the 3D vector onto the (y, z) plane such that $\Pi_{yz}([x, y, z]) = [0, y, z]$ to yield horizontal and vertical – but not torsional – pursuit. The pursuit system model computes an eye command e_{P}. The parameter values defining the smooth pursuit model are identical to those in (Robinson et al. 1986).

Appendix D: The velocity storage Integrator model

In the sensory weighting model, rotational and otolith information is combined to compute an intermediate estimate of head angular velocity as shown in (12). When the sensory estimate of gravity $\tilde{g}$ is not varying, its derivative $\mathrm{d}\tilde{g}/\mathrm{d}t$ is null and

$$\hat{\omega}_2 = \langle \tilde{\omega}, \tilde{g}^{\mathrm{P}} \rangle \tilde{g} \tag{D1}$$

With $\tilde{g} = [\tilde{g}_x, \tilde{g}_y, \tilde{g}_z]$, $\tilde{g}^{\mathrm{P}} = \left[\tilde{g}_x^{\mathrm{P}}, \tilde{g}_y^{\mathrm{P}}, \tilde{g}_z^{\mathrm{P}}\right]$, and using (D1) in (15), the central estimate of head angular velocity $\hat{\omega}$ can be expressed as follows:

$$\hat{\omega} = \mathbf{A}(\tilde{g}, \tilde{g}^{\mathrm{P}})\tilde{\omega} + W_{\omega,3}(\tilde{r} - \tilde{e}) \tag{D2}$$

$$\mathbf{A}(\tilde{g}, \tilde{g}^{\mathrm{P}}) = \begin{bmatrix} W_{\omega,1} + W_{\omega,2}\tilde{g}_x^{\mathrm{P}}\tilde{g}_x & W_{\omega,2}\tilde{g}_y^{\mathrm{P}}\tilde{g}_x & W_{\omega,2}\tilde{g}_z^{\mathrm{P}}\tilde{g}_x \\ W_{\omega,2}\tilde{g}_x^{\mathrm{P}}\tilde{g}_y & W_{\omega,1} + W_{\omega,2}\tilde{g}_y^{\mathrm{P}}\tilde{g}_y & W_{\omega,2}\tilde{g}_z^{\mathrm{P}}\tilde{g}_y \\ W_{\omega,2}\tilde{g}_x^{\mathrm{P}}\tilde{g}_z & W_{\omega,2}\tilde{g}_y^{\mathrm{P}}\tilde{g}_z & W_{\omega,1} + W_{\omega,2}\tilde{g}_z^{\mathrm{P}}\tilde{g}_z \end{bmatrix} \tag{D3}$$

Since non-diagonal elements are non-zero in the general case, cross-coupling should occur for various orientations. For roll tilts, the matrix $\mathbf{A}(\tilde{g}, \tilde{g}^{\mathrm{P}})$ is

$$\mathbf{A}(\tilde{g}, \tilde{g}^{\mathrm{P}}) = \begin{bmatrix} W_{\omega,1} & 0 & 0 \\ 0 & W_{\omega,1} + W_{\omega,2}\tilde{g}_y^{\mathrm{P}}\tilde{g}_y & W_{\omega,2}\tilde{g}_z^{\mathrm{P}}\tilde{g}_y \\ 0 & W_{\omega,2}\tilde{g}_y^{\mathrm{P}}\tilde{g}_z & W_{\omega,1} + W_{\omega,2}\tilde{g}_z^{\mathrm{P}}\tilde{g}_z \end{bmatrix} \tag{D4}$$

Therefore, when a subject is roll tilted, horizontal-to-vertical and vertical-to-horizontal cross-couplings are predicted by the sensory weighting model. For pitch tilts, the matrix $\mathbf{A}(\tilde{g}, \tilde{g}^{\mathrm{P}})$ is

$$\mathbf{A}(\tilde{g}, \tilde{g}^{\mathrm{P}}) = \begin{bmatrix} W_{\omega,1} + W_{\omega,2}\tilde{g}_x^{\mathrm{P}}\tilde{g}_x & 0 & W_{\omega,2}\tilde{g}_z^{\mathrm{P}}\tilde{g}_x \\ 0 & W_{\omega,1} & 0 \\ W_{\omega,2}\tilde{g}_x^{\mathrm{P}}\tilde{g}_z & 0 & W_{\omega,1} + W_{\omega,2}\tilde{g}_z^{\mathrm{P}}\tilde{g}_z \end{bmatrix} \tag{D5}$$

Therefore, when a subject is pitched, horizontal-to-torsional and torsional-to-horizontal cross-couplings are predicted by the sensory weighting model. If the idiotropic vector $\tilde{g}^{\mathrm{M}} = [0, 0, -1]$ replaces the vector $\tilde{g}^{\mathrm{P}}$ in (D3)

$$\mathbf{A}(\tilde{g}, \tilde{g}^{\mathrm{M}}) = \begin{bmatrix} W_{\omega,1} & 0 & -W_{\omega,2}\tilde{g}_x \\ 0 & W_{\omega,1} & -W_{\omega,2}\tilde{g}_y \\ 0 & 0 & W_{\omega,1} + W_{\omega,2}\tilde{g}_z \end{bmatrix} \tag{D6}$$

In that case, only horizontal-to-vertical and horizontal-to-torsional cross-couplings would be predicted.

References

Anderson JH, Blanks RH, Precht W (1978) Response characteristics of semicircular canal and otolith systems in cat. I. Dynamic responses of primary vestibular fibers. Exp Brain Res 32: 491–507

Angelaki D, Hess B (1994) Inertial representation of angular motion in the vestibular system of rhesus monkeys. I. Vestibulo-ocular reflex. J Neurophysiol 71: 1222–1249

Angelaki D, Hess B (1995) Inertial representation of angular motion in the vestibular system of rhesus monkeys. II. Otolith-controlled transformation that depends on an intact cerebellar nodulus. J Neurophysiol 73: 1729–1751

Angelaki D, McHenry M, Dickman J, Newlands S, Hess B (1999) Computation of inertial motion: neural strategies to resolve ambiguous otolith information. J Neurosci 19: 316–327

Barnes GR (1993) Visual–vestibular interaction in the control of head and eye movement:the role of visual feedback and predictive mechanisms. Prog Neurobiol 41: 435–472

Benson A, Bodin M (1966a) Comparison of the effect of the direction of the gravitational acceleration on post-rotational responses in yaw, pitch, and roll. Aerosp Med 37: 889–897

Benson A, Bodin M (1966b) Interaction of linear and angular accelerations on vestibular receptors in man. Aerosp Med 37: 144–154

Black FO, Wade SW, Nashner LM (1996) What is the minimal vestibular function required for compensation? Am J Otol 17: 410–409

Borah J, Young LR, Curry RE (1988) Optimal estimator model for human spatial orientation. Ann N Y Acad Sci 545: 1–73

Busettini C, Miles F, Schwarz U, Carl J (1994) Human ocular responses to translation of the observer and of the scene: dependence on viewing distance. Exp Brain Res 100: 484–494

Cohen B, Henn V, Raphan T, Dennett D (1981) Velocity storage, nystagmus and visual-vestibular interactions in humans. Ann N Y Acad Sci 374: 421–433

Cohen B, Suzuki JI, Raphan T (1983) Role of the otolith organs in generation of horizontal nystagmus: effects of selective labyrinthine lesions. Brain Res 276: 159–64

Correia M, Money K (1970) The effect of blockage of all six semicircular canal ducts on nystagmus produced by dynamic linear acceleration in the cat. Acta Otolaryngol 69: 7–16

Curthoys I, Blanks R, Markham C (1977) Semicircular canal functional anatomy in cat, guinea pig and man. Acta Otolaryngol 83: 258–265

Dai M, Raphan T, Cohen B (1991) Spatial orientation of the vestibular system: dependence on optokinetic after-nystagmus on gravity. J Neurophysiol 66: 1422–1439

Darlot C (1993) The cerebellum as a predictor of neural messages – I. The stable estimator hypothesis. Neuroscience 56: 617–646
Darlot C, Cohen B, Berthoz A, Denise P (1987) Eye movements and perceptual effects induced by off-vertical axis rotation at small angles of tilt. In: Graham M, Kemink J (eds) The vestibular system: neurophysiologic and clinical research. Raven, New York, pp 271–280
Darlot C, Denise P, Droulez J, Cohen B, Berthoz A (1988) Eye movements induced by off-vertical axis rotation (OVAR) at small angles of tilt. Exp Brain Res 73: 91–105
Darlot C, Zupan L, Etard O, Denise P, Maruani A (1996) Computation of inverse dynamics for the control of movements. Biol Cybern 75: 173–186
Denise P, Darlot C (1993) The cerebellum as a predictor of neural messages – I. Role in motor control and motion sickness. Neuroscience 56: 647–655
Denise P, Darlot C, Droulez J (1988) Motion perceptions induced by off-vertical axis rotation (OVAR) at small angles of tilt. Exp Brain Res 73: 106–114
Dichgans J, Held R, Young LR, Brandt T (1972) Moving visual scenes influence the apparent direction of gravity. Science 178: 1217–1219
Droulez J, Cornilleau-Pérès V (1993) Application of the coherence scheme to the multisensory fusion problem. In: Berthoz A (ed) Multisensory control of movement. Oxford University Press, Oxford, pp 485–501
Droulez J, Darlot C (1989) The geometric and dynamic implications of the coherence constraints in three-dimensional sensorimotor interactions. In: Jeannerod M (ed) Attention and performance XIII. Erlbaum, New York, pp 495–526
Ferman L, Collewijn H, Jansen TC, Van den Berg AV (1987) Human gaze stability in the horizontal, vertical and torsional direction during voluntary head movements, evaluated with a three-dimensional scleral induction coil technique. Vision Res 27: 811–828
Fernandez C, Goldberg J (1971) Physiology of peripheral neurons innervating semicircular canals of the squirrel monkey. II. Response to sinusoidal stimulation and dynamics of peripheral vestibular system. J Neurophysiol 34: 661–675
Fernandez C, Goldberg J (1976a) Physiology of peripheral neurons innervating the otolith organs of the squirrel monkey. I. Response to static tilts and to long-duration centrifugal force. J Neurophysiol 39: 970–984
Fernandez C, Goldberg J (1976b) Physiology of peripheral neurons innervating the otolith organs of the squirrel monkey. III. Response dynamics. J Neurophysiol 39: 996–1008
Fetter M, Tweed D, Hermann W, Wohland-Braun B, Koenig E (1992) The influence of head position and head reorientation on the axis of eye rotation and the vestibular time constant during postrotatory nystagmus. Exp Brain Res 91: 121–128
Fetter M, Heimberger J, Black R, Hermann W, Sievering F, Dichgans J (1996) Otolith-semicircular canal interaction during postrotatory nystagmus in humans. Exp Brain Res 108: 463–472
Fredrickson J, Schwartz D (1979) Vestibulo-cortical projections. In: Naunton R (ed) The vestibular system. Academic, New York, pp 203–210
Fuchs AF, Scudder CA, Kaneko CR (1988) Discharge patterns and recruitment order of identified motoneurons and internuclear neurons in the monkey abducens nucleus. J Neurophysiol 60: 1874–95
Gizzi M, Raphan T, Rudolph S, Cohen B (1994) Orientation of human optokinetic nystagmus to gravity: a model-based approach. Exp Brain Res 99: 347–360
Glasauer S (1992) Interaction of semicircular canals and otoliths in the processing structure of the subjective zenith. Ann N Y Acad Sci 656: 847–849
Glasauer S (1993) Human spatial orientation during centrifuge experiments: Non-linear interaction of semicircular canals and otoliths. In: Krejcova H, Jerabek J (eds) Proceedings of the 17th Barany Society Meeting, Prague, Czech Republic, 1–5 June pp. 48–52
Glasauer S, Merfeld D (1997) Modeling three-dimensional vestibular responses during complex motion stimulation. In: Fetter M, Haswanter T, Misslich H, Tweed D (eds) Three-dimensional kinematics of eye, head and limb movements. Harwood, Reading, pp 387–398
Goldberg J, Fernandez C (1982) Eye movements and vestibular-nerve responses produced in the squirrel monkey by rotations about an earth-horizontal axis. Exp Brain Res 46: 393–402
Graf W, Simpson JI, Leonard CS (1988) Spatial organization of visual messages of the rabbit's cerebellar flocculus. II. Complex and simple spike responses of Purkinje cells. J Neurophysiol 60: 2091–2121
Guedry F (1965) Orientation of the rotation-axis relative to gravity: its influence on nystagmus and the sensation of rotation. Acta Otolaryngol 60: 30–49
Hain TC (1986) A model of the nystagmus induced by off vertical axis rotation. Biol Cybern 54: 337–350
Harris L, Barnes G (1987) Orientation of vestibular nystagmus is modified by head tilt. In: Graham M, Kemink J (eds) The vestibular system: neurophysiologic and clinical research. Raven , New York, pp 539–548
Haslwanter T, Jaeger R, Mayr S, Fetter M (2000) Three-dimensional eye-movement responses to off-vertical axis rotations in humans. Exp Brain Res 134: 96–106
Hildebrand FB (1976) Advanced calculus for applications, 2nd ed. Prentice-Hall, Englewood Cliffs, NJ, pp 53–80
Howard IP (1997) Interactions within and between the spatial senses. J Vestib Res 7: 311–345
Jaggi-Schwarz K, Misslisch H, Hess BJ (2000) Canal-otolith interactions after off-vertical axis rotations I. Spatial reorientation of horizontal vestibuloocular reflex. J Neurophysiol 83: 1522–35
Jell R, Ireland D, Lafortune S (1984) Human optokinetic afternystagmus. Slow-phase characteristics and analysis of the decay of slow phase velocity. Acta Otolaryngol 98: 462–471
Kawato M, Furukawa K, Suzuki R (1987) A hierarchical neural-network model for control and learning of voluntary movement. Biol Cybern 57: 169–185
Koenig E, Allum JHJ, Dichgans J (1978) Visual-vestibular interaction upon nystagmus slow phase velocity in man. Acta Otolaryngol 85: 397–410
Krapp HG, Hengstenberg R (1996) Estimation of self-motion by optic flow processing in single visual interneurons. Nature 384: 463–466
Lafortune S, Ireland D, Jell R, DuVal L (1986) Human optokinetic afternystagmus. Stimulus velocity dependence of the two-component decay model and involvement of pursuit. Acta Otolaryngol 1010: 183–192
Lansberg M, Guedry F, Graybiel A (1965) Effect of changing resultant linear acceleration relative to the subject on nystagmus generated by angular acceleration. Aerosp Medicine 36: 456–460
Loe PR, L TD, Werner G (1973) The neural signal of angular head position in primary afferent vestibular nerve axons. J Physiol (Lond) 230: 29–50
Mayne R (1974) A systems concept of the vestibular organs. In: Kornhuber H (ed) Handbook of Sensory Physiology, vol VI. vestibular system, part 2: psychophysics, applied aspects and general interpretations. Springer, Berlin Heidelberg New York, pp 493–580
Melvill Jones G, Barry W, Kowalsky N (1964) Dynamics of the semicircular canals compared in yaw, pitch, and roll. Aerosp Medicine 35: 984–989
Merfeld DM (1990) Spatial orientation in the squirrel monkey: an experimental and theoretical investigation. PhD thesis, Massachusetts Institute of Technology, Cambridge, Mass.
Merfeld DM (1995a) Modeling human vestibular responses during eccentric rotation and off vertical axis rotation. Acta Otolaryngol Suppl 520: 354–359
Merfeld DM (1995b) Modeling the vestibulo-ocular reflex of the squirrel monkey during eccentric rotation and roll tilt. Exp Brain Res 106: 123–134

Merfeld DM, Young LR (1995) The vestibulo-ocular reflex of the squirrel monkey during eccentric rotation and roll tilt. Exp Brain Res 106: 111–122

Merfeld DM, Wearne S, Curthoys I, Halmagyi G (1992) Perceptual tilt responses in humans during eccentric rotation. In: Krejcova H, Jerabek J (eds) Proceedings of the 17th Barany Society Meeting, Prague, Czech Republic, 1–5 June, pp 73–74

Merfeld DM, Young L, Oman C, Shelhamer M (1993a) A multidimensional model of the effect of gravity on the spatial orientation of the monkey. J Vestib Res 3: 141–161

Merfeld DM, Young L, Paige G, Tomko D (1993b) Three dimensional eye movements of squirrel monkeys following post rotatory tilt. J Vestib Res 3: 123–139

Merfeld DM, Zupan L, Peterka RJ (1999) Humans use an internal model to separate gravity and linear acceleration. Nature 398: 615–618

Merfeld DM, Zupan LH, Gifford CA (2001) Neural processing of gravito-inertial cues in humans. II. Influence of the semicircular canals during eccentric rotation. J Neurophysiol 85: 1648–1660

Mergner T, Glasauer S (1999) A simple model of vestibular canal-otolith signal fusion. Ann N Y Acad Sci 871: 430–4

Mergner T, Huber W, Becker W (1997) Vestibular-neck interaction and transformation of sensory coordinates. J Vestib Res 7: 347–367

Minor L, Goldberg J (1991) Vestibular-nerve inputs to the vestibulo-ocular reflex: a functional-ablation study in the squirrel monkey. J Neurosci 11: 1636–1648

Minor LB, Lasker DM, Backous DD, Hullar TE (1999) Horizontal vestibuloocular reflex evoked by high-acceleration rotations in the squirrel monkey. I. Normal responses. J Neurophysiol 82: 1254–70

Mittelstaedt H (1983) A new solution to the problem of the subjective vertical. Naturwissenschaften 70: 272–281

Mittelstaedt H (1986) The subjective vertical as a function of visual and extraretinal cues. Acta Psycol (Amst) 63: 63–85

Mittelstaedt H, Glasauer S, Gralla G, Mittelstaedt M (1989) How to explain a constant subjective vertical at constant high speed rotation about an earth-horizontal axis. Acta Otolaryngol 468: 295–299

Oman CM (1982) A heuristic mathematical model for the dynamics of sensory conflict and motion sickness. Acta Otolaryngol Suppl 392: 1–44

Ormsby CC, Young LR (1977) Integration of semicircular canal and otolith information for multisensory orientation stimuli. Math Biosci 34: 1–21

Paige G (1989) The influence of target distance on eye movement responses during vertical linear motion. Exp Brain Res 77: 585–593

Paige G, Tomko D (1991) Eye movement responses to linear head motion in the squirrel monkey. I. Basic characteristics. J Neurophysiol 65: 1170–1182

Raphan T, Sturm D (1991) Modeling the spatiotemporal organization of velocity storage in the vestibuloocular reflex by optokinetic studies. J Neurophysiol 66: 1410–1421

Raphan T, Matsuo V, Cohen B (1977) A velocity storage mechanism responsible for optokinetic nystagmus (OKN), optokinetic after-nystagmus (OKAN) and vestibular nystagmus. In: Baker R, Berthoz A (eds) Control of gaze by brain stem neurons, developments in neuroscience. Elsevier, Amsterdom, pp 37–47

Robinson D (1977) Vestibular and optokinetic symbiosis: an example of explaining by modeling. In: Baker R, Berthoz A (eds) Control of gaze by brain stem neurons, developments in neuroscience. Elsevier, Amsterdom, pp 49–58

Robinson D, Gordon J, Gordon S (1986) A model of the smooth pursuit eye movement system. Biol Cybern 55: 43–57

Schmid R, Zambarbieri D, Sardi R (1979) A mathematical model of the optokinetic reflex. Biol Cybern 34: 215–25

Schmid R, Buizza A, Zambarbieri D (1980) A non-linear model for visual-vestibular interaction during body rotation in man. Biol Cybern 36: 143–51

Schwarz C, Miles F (1991) Ocular responses to translation and their dependence on viewing distance. I. Motion of the observer. J Neurophysiol 66: 851–864

Schwarz C, Busettini C, Miles F (1989) Ocular responses to linear motion are inversely proportional to viewing distance. Science 245: 1394–1396

Simpson JI (1984) The accessory optic system. Annu Rev Neurosci 7: 13–42

Spiegel M (1972) Moving coordinate systems. In: Theory and problems of theoretical mechanics with an introduction to Lagrange's equations and Hamiltonian theory. Schaum, New York, pp 144–159

Stockwell C, Guedry F (1970) The effect of semicircular canal stimulation during tilting on the subsequent perception of the visual vertical. Acta Otolaryngol 70: 170–175

Tomko D, Paige G (1992) Linear vestibuloocular reflex during motion along axes between nasooccipital and interaural. Ann N Y Acad Sci 656: 233–241

Udo de Haes H (1970) Stability of apparent vertical and ocular countertorsion as a function of lateral tilt. Percept Psychophys 8: 137–142

Viirre E, Tweed D, Milner K, Vilis T (1986) A reexamination of the gain of the vestibulo ocular reflex. J Neurophysiol 56: 439–450

Von Holst E, Grisebach E (1951) Einfluss des Bogengangsystems auf die "subjektive Lotrechte" bein Menschen. Naturwissenschaften 38: 67–68

Von Holst E, Mittelstaedt H (1950) Das Reafferenzprinzip (Wechselwirkungen zwischen Zentralnervensystem und Peripherie). Naturwissenschaften 37: 464–76

Waespe W, Henn V (1977) Neuronal activity in the vestibular nuclei of the alert monkey during vestibular and optokinetic stimulation. Exp Brain Res 27: 523–538

Waespe W, Henn V (1979) The velocity response of vestibular nucleus neurons during vestibular, visual, and combined angular acceleration. Exp Brain Res 37: 337–47

Wall C III, Furman J (1990) Visual-vestibular interaction in humans during earth-horizontal axis rotation. Acta Otolaryngol 109: 337–344

Wall C III, Merfeld DM, Zupan L (1999) Effects of static orientation upon human optokinetic afternystagmus. Acta Otolaryngol 119: 16–23

Wearne S, Raphan T, Cohen B (1996) Nodulo-uvular control of central vestibular dynamics determines spatial orientation of the angular vestibulo-ocular reflex. Ann N Y Acad Sci 781: 364–384

Wearne S, Raphan T, Cohen B (1998) Control of spatial orientation of the angular vestibulo ocular reflex by the nodulus and uvula. J Neurophysiol 79: 2690–2715

Wearne S, Raphan T, Cohen B (1999) Effects of tilt of the gravito-inertial acceleration vector on the angular vestibuloocular reflex during centrifugation. J Neurophysiol 81: 2175–2190

Wolpert D, Ghahramani Z, Jordan M (1995) An internal model for sensorimotor integration. Science 269: 1880–1882

Wylie DRW, Frost BJ (1993) Responses of pigeon vestibulocerebellar neurons to optokinetic stimulation. II. The 3-dimensional reference frame of rotation neurons in the flocculus. J Neurophysiol 70: 2647–2659

Wylie DRW, Bischof WF, Frost BJ (1998) Common reference frame for neural coding of translational and rotational optic flow. Nature 392: 278–282

Young LR, Meiry JL (1968) A revised dynamic otolith model. Aerosp Med 39: 606–608

Zupan LH (1995) Modélisation du Réflexe Vestibulo-Oculaire et Prédiction des Cinétoses. PhD, thesis Ecole Nationale Supérieure des Télé communications, suppress

Zupan LH, Droulez J, Darlot C, Denise P, Maruani A (1994) Modelization of the vestibulo-ocular reflex (VOR) and motion sickness prediction. In: Marinaro M, Morasso PG (eds) Proceedings of the International Conference on Artificial Neural Networks, Sorrento, Italy, 26–29 May, pp 106–109

Zupan LH, Peterka RJ, Merfeld DM (2000) Neural processing of gravito-inertial cues in humans. I. Influence of the semicircular canals following post-rotatory tilt. J Neurophysiol 84: 2001–15

Zupan LH, Merfeld DM, King K (2001) The influence of visual rotational cues on human orientation and eye movements. In: Proceedings of the 24th Annual ARO Midwinter Research Meeting, St. Petersburg, Fla